Water Conserv Sci Eng (2016) 1:21–48
DOI 10.1007/s41101-016-0002-2

ORIGINAL PAPER

Investigation on Elimination of As(III) and As(V) from Wastewater Using Bacterial Biofilm Supported on Sawdust/$MnFe_2O_4$ Composite

M. S. Podder[1] · **C. B. Majumder**[1]

Received: 10 October 2015 / Revised: 11 March 2016 / Accepted: 11 March 2016 / Published online: 2 May 2016

Abstract The goal of the present research was to study the ability of *Corynebacterium glutamicum* MTCC 2745 immobilized on Sawdust/$MnFe_2O_4$ composite to treat arsenic bearing wastewater by simultaneous biosorption and bioaccumulation (SBB) system at laboratory scale and also to investigate the influences of initial pH, biosorbent dose, contact time, temperature and initial arsenic concentration on biosorption/bioaccumulation of both As(III) and As(V). The surface texture of the immobilized bacterial cells was investigated through SEM–EDX analysis. The presence of functional groups on the surface of immobilized bacterial cells that may interact with the metal ion was confirmed by FT-IR. The pattern of biosorption/bioaccumulation fitted well with Vieth and Sladek isotherm model for As(III) and Brouers–Sotolongo and Fritz–Schlunder–V isotherm models for As(V). The maximum adsorption capacity estimated using Langmuir model was 1672.32214 mg/g for As(III) and 1861.71453 mg/g for As(V) at 30 °C temperature and 240 min contact time. The results showed that As(III) and As(V) removal was strongly pH-dependent with an optimum pH value of 7.0. The effect of co-existing ions, such as Cu^{2+}, Zn^{2+}, Bi^{3+}, Cd^{2+}, Fe^{3+}, Pb^{2+}, Co^{2+}, Ni^{2+}, Cr^{6+} and SO_4^{2-}, at different concentrations were examined. Desorption study exhibited that over 81.34 and 88.727 % could be desorbed from immobilized bacterial cells with 0.05 M NaOH solution.

Keywords As(III) and As(V) · SD/$MnFe_2O_4$ composite · Optimization · Simultaneous biosorption and bioaccumulation · Equilibrium isotherm

Introduction

Arsenic is one of endocrine disruptors and is classified as one of the most toxic and carcinogenic chemical element [1, 2]. Arsenic occurrence in the environment can be because of human activities such as smelting of non-ferrous metals, uses of arsenical pesticides, insecticides, mining and burning of fossil fuels [3]. Copper smelting produces a huge volume of wastewater having large amounts of highly carcinogenic metalloid like arsenic species, poses a serious threat towards man and the flora and fauna of our ecosystem contaminating the natural water tables (ground water and surface water) in the vicinity [4]. With the aim of maintaining a good quality of fresh water resources, this wastewater must be treated so that the water can be reverted to the ecosystems. As(III) and As(V) ions are the most common arsenic species in nature and create the extreme environmental issue [5]. On the basis of investigation of the detrimental effect of arsenic on human body, in drinking water, the maximum contaminant level (MCL) of arsenic has been revised to 10 from 50 μg/L by the World Health Organization (WHO) in 1993 [6] and the European Commission in 2003 [7].

New and very old techniques used to remove arsenic from have been developed including precipitation [8], electrochemical treatment [4], electrocoagulation [5] and adsorption [9]. However, these high-technology methods have considerable

Electronic supplementary material The online version of this article (doi:10.1007/s41101-016-0002-2) contains supplementary material, which is available to authorized users.

✉ M. S. Podder
mou.chem11@gmail.com

C. B. Majumder
cbmajumder@gmail.com

[1] Department of Chemical Engineering, Indian Institute of Technology, Roorkee 247667, India

drawbacks such as high capital and operational cost, high reagent or energy necessities, production of contaminated sludge that require disposal and are not appropriate for small-scale industries and are not eco-friendly [10, 11]. Among several treatment techniques, the surface modified adsorbents and biological treatment with living microbes are gaining interest in recent years for the removal of arsenic from contaminated water [3]. Biological method has many benefits over the chemical ones in the aspects of environmental friendliness, ease in application, more effectiveness and cost reduction [12]. Most of the researches have focused on either the biosorption of metal ion on the surface of non-living biomass or biosorption on the surface living microbial cells followed by intracellular and extracellular accumulation of metal ion [13]. Giri et al. reported the unexploited sorption properties of the *Bacillus cereus* for the removal of As(III) from aqueous solutions [14, 15]. Recently, studies related to biosorption of arsenic from aqueous solution by *Mougeotia genuflexa* [16], *Rhodococcus sp.* WB-12 [17], *Arthrobacter* sp. [18] were carried out.

A novel technique for an efficient metal ion removal mediated by immobilized bacterial cells is designed. This metal ion removal system is called simultaneous biosorption and bioaccumulation (SBB) system. In this system, both non-living biomass and living microbial cells are used simultaneously. Due to practical difficulties in solid–liquid separation, the free biomass is immobilized on the support. Immobilized biomass also shows better potential in packed/fluidized bed reactors and continuous stirred tank reactors due to minimal clogging under continuous flow conditions as well as effective biosorbent regeneration and metal recovery [19]. A small number of researchers have investigated the simultaneous use of both non-living biomass and living microbial cells [20–23]. Mondal et al. described the bio-removal of arsenic from contaminated water by using *Ralstonia eutropha MTCC 2487* and activated carbon in batch reactor [20].

C. glutamicum MTCC 2745 species is of specific attention due to its high capability for abatement biologically. Bacteria can depollute arsenic wastewater, by accumulation outside the cells and/or biosorption of the ion on their surface [24] as was defined earlier for *E. coli* [25] and *Ralstonia eutropha* [26].

In the present work, a composite of Sawdust/$MnFe_2O_4$ was synthesized in order to hybridize high adsorption capacity of $MnFe_2O_4$ with biosorptivity of sawdust. So, the current study aimed at selection of arsenic resistant strain, followed by the immobilization of microbial strain on carrier particles (SD/$MnFe_2O_4$ composite), and use of immobilized microbial cells as biosorbent for the biosorption/bioaccumulation of arsenic (either As(III) or As(V)) ions from synthetic wastewater in batch studies. SD/$MnFe_2O_4$ composite was used as carrier because of its higher porosity, surface area, easy availability of sawdust and cost effectiveness. Sawdust is the agricultural waste which contains many organic compounds (cellulose, hemicellulose and lignin) with polyphenolic groups that might be beneficial to bind heavy metals ions [27]. The sawdust is also rich in hydroxyl groups like tannins [27]. The hydroxyl groups can offer chemical reaction sites and adsorb iron and manganese ions to grow $MnFe_2O_4$ particles. Formation of $MnFe_2O_4$ layer enhanced the net positive charge (NPC) of SD/$MnFe_2O_4$ composite and improved the arsenic biosorption capacity. The iron and manganese in SD/$MnFe_2O_4$ composite triggered the oxidation of As(III) to As(V), which can easily be adsorbed by the biosorbent in the experimental pH range [28]. In case of SD, As(III) did not oxidize to As(V). So, the binding of the As(III) or As(V) to the surface of SD/$MnFe_2O_4$ composite biosorbent generally resulted in higher binding capacities owing to the probable various electron transfers from either Mn or Fe ions [29].

Moreover, the aims were prolonged to investigate the effect of initial pH of the solution, biosorbent dose, contact time, temperature and initial concentrations of arsenic (either As(III) or As(V)) ions on the removal of arsenic ions from synthetic wastewater. The effect of co-existing ions present in copper smelting wastewater on the removal of arsenic (either As(III) or As(V)) was investigated. Desorption of arsenic-loaded *C. glutamicum* MTCC 2745 immobilized on surface of SD/$MnFe_2O_4$ composite was also examined. The second part of the present research was to study 30 adsorption isotherms for biosorption/bioaccumulation of both As(III) and As(V) on *C. glutamicum* MTCC 2745 immobilized on SD/$MnFe_2O_4$ composite to inspect their ability for modelling the biosorption/bioaccumulation equilibrium data.

Materials and Methods

Materials

Sawdust of *Syzygium cumini* (Jamun tree) was collected from timber working shop situated near the campus of Indian Institute of Technology, Roorkee, India. All the chemicals and reagents were of analytical reagent grade and used without additional purification. The stock solutions of As(III) and As(V) were prepared by dissolving sodium arsenite ($NaAsO_2$) and sodium arsenate (Na_2HAsO_4, $7H_2O$), purchased from Himedia Laboratories Pvt. Ltd. Mumbai India, in double distilled water, respectively. All other necessary chemicals used in the experiments were purchased from Himedia Laboratories Pvt. Ltd. Mumbai India.

Microorganism and Growth Medium

The microorganism used was the arsenic-resistant bacterium *C. glutamicum* MTCC 2745 (Microbial Type Culture Collection and Gene Bank (MTCC), Chandigarh, India). Culture media was prepared as per the guidelines of microbial type cell culture (MTCC). Composition of growth medium and cultivation conditions are shown in Table 1.

Table 1 Composition of growth medium and cultivation conditions

Component (g/L) or condition	
Beef extract	1.0
Yeast extract	2.0
Peptone	5.0
NaCl	5.0
pH	7.0
Temperature (°C)	30

Acclimatization

The revived culture was initially grown in MTCC prescribed growth media in a 250 mL round bottom flask tightly closed with cotton plug as follows:

C. glutamicum MTCC 2745 was cultivated in 250 mL flask containing 100 mL of the growth media with As(III) and As(V). The cultures were acclimatized to As(III) and As(V) individually exposing the culture in a series of shake flasks (Mondal et al., 2008) (The details provided with supplementary materials).

Methods

Biosorbent Preparation

Sawdust (SD) was washed to clean the adhering dirt, rinsed thoroughly with double distilled water and finally heated in an air oven at 105 °C for 4 h. Further details of biosorbent preparation are provided with the supplementary materials.

Immobilization of Microbial Cells Onto the Biosorbent

To immobilize *C. glutamicum* MTCC 2745 onto prepared SD/$MnFe_2O_4$ composite initially, 90-mL culture media was inoculated with 5 mL of bacterial suspension of *C. glutamicum* MTCC 2745 from both As(III) and As(V) acclimatized 24-h old culture. The flasks were incubated at 30 °C for another 24 h with moderate shaking at 120 rpm. Then, immobilization of bacterial cell was performed by adding weighed amount of prepared SD/$MnFe_2O_4$ composite to the above suspension containing 24-h old culture. Then, the flasks were again incubated at 30 °C for the next 24 h with moderate shaking at 120 rpm. Bacterial cell immobilization was established by observing a small amount of bacterial treated SD/$MnFe_2O_4$ composite through scanning electron microscopy.

Characterization

Infrared spectra of the unloaded and metal loaded SD/$MnFe_2O_4$ composite attached with biofilm were obtained using a Fourier transform infrared spectrometer (NICHOLET 6700, coupled with OMNIC software version 6.2). The measurements of SEM were carried out for noticing the surface morphologies of the SD/$MnFe_2O_4$ composite attached with biofilm before and after biosorption/bioaccumulation process (SEM; LEO Electron Microscopy, England). The images were taken with an accelerator voltage = 15 kV and an emission current = 100 μA by the Tungsten filament.

Batch Experimental Studies and Analytical Methods

A medium with 1.0 g/L of beef extract and 2.0 g/L of yeast extract, 5.0 g/L of peptone and 5.0 g/L of NaCl was utilized for the growth of the microorganism. The media was sterilized at 121 °C for 15 min, cooled to room temperature, inoculated with bacteria and kept at 30 °C for 24 h with moderate shaking (120 rpm) in an incubator cum orbital shaker (REMI Laboratory instruments). Batch biosorption/bioaccumulation studies for optimizing process parameters were performed in round bottom flasks by taking 100 mL of *C. glutamicum* MTCC 2745 bacterial suspension as a test solution in 250 mL round bottom flask closed with cotton plug tightly. After 24 h of immobilization of bacteria on SD/$MnFe_2O_4$ composite as described above, the effect of difference process parameters (such as pH, biosorbent dose, contact time, temperature and initial adsorbate (As(III) or As(V)) concentration) were studied adding calculated amount of arsenic (As(III) or As(V)). To regulate the initial pH of the solution using a digital pH metre (HACH® India), 1.0 N NaOH and 1.0 N HCl solutions were used. The flasks were moderately agitated in an incubator cum orbital shaker (REMI Laboratory instruments) working at 120 rpm. The standard experimental operating conditions for batch SBB studies are exhibited in Table 2.

The samples were withdrawn from the flasks through filtration by Whatman Filter paper (Cat No 1001 125) at predetermined time intervals and then centrifuged at 10,000 rpm for 10 min and then centrifuged at 10,000 rpm for 10 min (Remi Instruments ltd., Mumbai India) for studying the influence of parameters and at equilibrium time for isotherm studies, a portion of filtrate was diluted with HNO_3 solution (10 %, *v*/*v*). The filtrate was analysed for determination of arsenic concentration using ThermoFisher Scientific iCE 3000 Series AA graphite furnace atomic absorption (GFAA) spectrometer (The details are provided with supplementary material).

With the purpose of estimating biosorption capacity, expressed as the amount of adsorbate molecules adsorbed per unit mass of adsorbent (mg/g), the adsorption capacity was calculated as follows:

$$q_e = (C_o - C_e)\frac{V}{m} \quad (3)$$

Table 2 Different process conditions used in this study

Type of experiments	Range of operating parameters				
	pH	Biosorbent dose (g/L)	Contact time (min)	Temperature (°C)	Initial concentration of As(III) or As(V) (mg/L)
Effect of pH	2.0–12.0	4	90	30	50
Effect of adsorbent dose	7.0	10	90	30	50
Effect of contact time	7.0	1	5–500	30	50
Effect of temperature	7.0	1	240	20–50	50
Effect of initial arsenic concentration	7.0	1	240	30	50–2000

The amount of adsorbate molecules adsorbed in terms of percentage was calculated as follows:

$$R_e(\%) = \frac{(c_o - c_e)}{c_o} \times 100 \quad (4)$$

Distribution coefficient R_d (L/g) was estimated using the mass balance equation as follows:

$$R_d = \frac{\text{Amount of adsorbate in adsorbent}}{\text{Amount of adsorbate in solution}} \times \frac{V}{M} \quad (5)$$

Interference Studies

The As(III) and As(V) binding capacity experiments were again done with synthetically prepared wastewater containing the co-existing ions commonly existing in copper smelting wastewater with arsenic solution. The effect of ions such as Cu^{2+}, Zn^{2+} and SO_4^{2-} (100–2000 mg/L), Fe^{3+}, Cd^{2+} and Bi^{3+} (10–500 mg/L), Pb^{2+}, Co^{2+}, Ni^{2+} and Cr^{6+} (1–70 mg/L) on elimination of As(III) and As(V) were inspected.

Desorption Studies

The desorption study was performed with As(III) and As(V) ions. The biosorption/bioaccumulation study was accomplished following the similar procedure stated above. Then again, desorption was examined as follows: 0.1 g of the arsenic–laden *C. glutamicum* MTCC 2745 immobilized on SD/$MnFe_2O_4$ composite from the previous metal biosorption/bioaccumulation study was added into a 250-mL round bottom flask containing 100 mL of different concentrations of NaOH (0, 0.001, 0.01, 0.05, 0.1, 0.5 and 1 M). The mixture was then agitated with the incubator cum orbital shaker at 120 rpm for 240 min at 30 °C. Then, the suspension solutions were filtered and analyzed for As(III) and As(V) according to the method discussed earlier. After the desorption experiment, the amount of desorbed As(III) and As(V) was estimated by the residual As(III) and As(V) concentrations in the solution. The amounts desorbed of adsorbate were assessed using the following equation:

$$\%\text{Desorption} = \frac{\text{Released adsorbate}\left({}^{\text{mg}}/_{\text{L}}\right)}{\text{Initially adsorbate adsorbed}\left({}^{\text{mg}}/_{\text{L}}\right)} \times 100 \quad (6)$$

Theoretical Background

Isotherm Studies

The capacity of the adsorption isotherm is essential and takes a governing part to determine the maximum capacity of adsorption. Mainly, it is a vital curve which defines the phenomenon that leading the retaining/discharge or movement of an adsorbate from liquid phase to solid adsorbent surface at a constant pH and temperature. It also offers a view of the process taken by the system under the study in a brief form, signifying how competently an adsorbent will adsorb and permits an estimation of the financial feasibility of the adsorbent, commercial applications for the definite adsorbent. When adsorbents containing solution has been kept in contact with the adsorbate for enough contact time and the concentration of adsorbate in the solution becomes constant, then adsorption equilibrium is achieved. Obviously, the statistical correlation playing a significant role in the isotherm modelling, operative designing and significant exercise of the adsorption systems, is observed by graphical representation of the uptake capacity of adsorbent against residual concentration of adsorbate. It is essential to form the utmost suitable correlation for equilibrium data with model predictions for optimizing the design for arsenic adsorption

Table 3 Adsorption isotherm models

Sr. no.	Expression	Equation form	Remarks
Single parameter model			
1	Henry's law	$q_e = K_{HE} C_e$	Simple expression
Two-parameter model			
2	Langmuir	$q_e = \frac{q_{mL} K_L C_e}{1 + K_L C_e}$	Monolayer adsorption
3	Freundlich	$q_e = K_F C_e^{\frac{1}{n_F}}$	Simple expression
4	Temkin	$q_e = \frac{RT}{b_{TE}} \ln(K_{TE} C_e) = B_{TE} \ln(K_{TE} C_e)$	Considering temperature
5	Dubinin–Radushkevich	$q_e = q_{mDR} \exp\left\{-K_{DR}\left[RT \ln\left(1 + \frac{1}{C_e}\right)\right]^2\right\}$	Considering temperature
6	Activated sludge	$q_e = K_m \left(\frac{C_e}{M}\right)^{\frac{1}{N_m}}$	Considering tendency of floc formation
7	Jovanovic	$q_{mJV}\{1 - \exp(-K_{JV} C_e)\}$	Adsorbent surface coverage is presumed to be zero
Three-parameter model			
8	Redlich–Peterson	$q_e = \frac{K_{RP} C_e}{1 + \alpha_{RP} C_e^{\beta_{RP}}}$	Approaches Freundlich at high concentration
9	Sips	$q_e = \frac{K_s q_{mS} C_e^{\frac{1}{mS}}}{1 + K_S C_e^{\frac{1}{mS}}}$	Approaches Langmuir at high concentration
10	Toth	$q_e = \frac{q_{mT} K_T C_e}{(1 + (K_T C_e)^{n_T})^{\frac{1}{n_T}}}$	Complicated
11	Brouers–Sotolongo	$q_e = q_{mBS}(1 - \exp(-K_{BS} C_e^{\alpha}))$	Complicated
12	Vieth–Sladek	$q_e = K_{VS} C_e + \frac{q_{mVS} \beta_{VS} C_e}{1 + \beta_{VS} C_e}$	Complicated
13	Koble–Corrigan	$q_e = \frac{A_{KC} B_{KC} C_e^{n_{KC}}}{1 + B_{KC} C_e^{n_{KC}}}$	Combination of both Freundlich and Langmuir
14	Khan	$q_e = \frac{q_{mK} b_K C_e}{(1 + b_K C_e)^{\alpha_K}}$	Approaches Freundlich at high concentration
15	Hill	$q_e = \frac{q_{mH} C_e^{n_H}}{K_H + C_e^{n_H}}$	Complicated
16	Jossens	$q_e = \frac{K_J C_e}{1 + J C_e^{b_J}}$	Approaches Henry's law at low capacities
17	Fritz–Schlunder–III	$q_e = \frac{q_{mFS} K_{FS} C_e}{1 + K_{FS} C_e^{n_{FS}}}$	Approaches Freundlich at high concentration
18	Unilan	$q_e = \frac{q_{mU}}{2s} \ln\left\{\frac{1 + K_U C_e \exp(s)}{1 + K_U C_e \exp(-s)}\right\}$	restricted to Henry's law
19	Holl–Krich	$q_e = \frac{q_{mHK} K_{HK} C_e^{nHK}}{1 + K_{HK} C_e^{nHK}}$	Approaches Langmuir at high concentration
20	Langmuir–Freundlich	$q_e = \frac{q_{mLF} (K_{LF} C_e)^{mLF}}{1 + (K_{LF} C_e)^{mLF}}$	Combination of both Freundlich and Langmuir
21	Langmuir–Jovanovic	$q_e = \frac{q_{mLJ} C_e \left\{1 - \exp\left(K_{LJ} C_e^{n_{LJ}}\right)\right\}}{1 + C_e}$	Combination of both Langmuir and Jovanovic
22	Jovanovic–Freundlich	$q_e = q_{mJF}(1 - \exp\{(-K_{JF} C_e)^{n_{JF}}\})$	Combination of both Freundlich and Jovanovic
23	Radke–Prausnitz I	$q_e = \frac{q_{mRPI} K_{RPI} C_e}{(1 + K_{RPI} C_e^{m_{RPI}})}$	Approaches Freundlich at high concentration
24	Radke–Prausnitz II	$q_e = \frac{q_{mRPII} K_{RPII} C_e}{1 + K_{RPII} C_e^{mRPII}}$	Approaches Freundlich at high concentration
25	Radke–Prausnitz III	$q_e = \frac{q_{mRPIII} K_{RPIII} C_e^{m_{RPIII}-1}}{1 + K_{RPIII} C_e^{m_{RPIII}-1}}$	Approaches Langmuir at high concentration for Radke–Prausnitz III.
26	Langmuir–Freundlich–Jovanovic	$q_e = \frac{q_{mLFJ} C_e^{n_{LFJ}} \{1 - \exp(-(K_{LFJ} C_e)^{n_{LFJ}})\}}{1 + C_e^{n_{LFJ}}}$	Combination of Langmuir, Freundlich and Jovanovic

Table 3 (continued)

Sr. no.	Expression	Equation form	Remarks
Four-parameter model			
27	Marczewski–Jaroniec	$q_e = q_{mMJ}\left(\frac{(K_{MJ}C_e)^{\frac{m_{MJ}}{n_{MJ}}}}{1+(K_{MJ}C_e)^{nMJ}}\right)^{\frac{m_{MJ}}{n_{MJ}}}$	Complicated
28	Baudu	$q_e = \frac{q_{mB}b_B C_e^{(1+x+y)}}{1+b_B C_e^{(1+x)}}$	Complicated
29	Fritz–Schlunder–IV	$q_e = \frac{A_{FS}C_e^{\alpha FS}}{1+B_{FS}C_e^{bFS}}$	Approaches Freundlich at high concentration
Five-parameter model			
30	Fritz–Schlunder–V	$q_e = \frac{q_{mFS5}K_1 C_e^{\alpha FS}}{1+K_2 C_e^{\beta FS}}$	Approaches Freundlich at high concentration

onto the adsorbent. Several empirical models including 1, 2, 3, 4 or even 5 parameters have been applied to fit batch equilibrium isotherm curves to biosorbents. To describe the adsorption equilibrium, numerous isotherm models were recommended (Table 3). The details of isotherm study are provided with supplementary materials along with Table S1.

Determining Adsorption Isotherm Parameters by Non-Linear Regression

The isotherm parameter sets are calculated by non-linear regression owing to the inherent bias resulting after linearization. This offers a mathematically laborious method to estimate isotherm parameters using the original isotherm equation [30, 31]. Mostly, Gauss–Newton methods or Levenberg–Marquardt based algorithms [32, 33] are used. As non-linear equations, the linearization step of the isotherm models leads to the modification of the distribution of error after converting the data to a linear form [30]. The equilibrium data for biosorption/bioaccumulation of arsenic on *C. glutamicum* MTCC 2745 immobilized on the surface of SD/$MnFe_2O_4$ composite were analysed by non-linear curve fitting analysis using professional graphics software package OriginPro (8.5.1 version) for fitting the one-, two-, three-, four- and five-parameter isotherm models.

The optimization method needs the choice of a Goodness-of-Fit Measure (GoFM) with the purpose of estimating the fitting of the isotherm to the experimental data. In the present research, six GoFM (residual sum of squares (SSE), reduced chi-square test (Reduced χ^2), coefficient of determination (R^2), adjusted R-square ($\overline{R^2}$), R value (R) and Root–MSE value) were employed for estimating isotherm parameters using the OriginPro software by considering 95 % confidence interval (The details provided with supplementary materials).

Results and Discussions

Characterization

FT-IR Analysis

The Fourier transform infrared spectra (FT-IR) study of fresh SD/$MnFe_2O_4$ composite as well as As(III) acclimatized *C. glutamicum* MTCC 2745 immobilized on surface of SD/$MnFe_2O_4$ composite at unloaded (represented by red shift) and metal loaded stage (represented by blue shift) (Fig. 1a; Table S2 and fresh SD/$MnFe_2O_4$ composite plus As(V) acclimatized *C. glutamicum* MTCC 2745 immobilized on surface of SD/$MnFe_2O_4$ composite at unloaded (represented by red shift) and metal loaded stage (represented by blue shift) (Fig. 1b; Table S3) at optimized batch experimental condition were observed for identifying the function groups responsible mainly for the process of biosorption/bioaccumulation. Surface –OH and –NH groups were main active functional groups liable for biosorption/bioaccumulation as the wavenumber shifted from 3432.725 to 3426.977 cm^{-1} (As(III)) and from 3434.653 to 3431.938 cm^{-1} (As(V)) which may be perhaps due to the complexation of –OH groups with As(III) or As(V) ions [34, 35]. Aliphatic C–H stretching may be responsible for biosorption/bioaccumulation of As(III) and As(V) on immobilized bacterial cells as wavenumber shifted from 2919.68992 to 2924.651 cm^{-1} and from 2921.673 cm^{-1} to 2925.271 cm^{-1}, respectively, possibly due to the complexation of C–H stretching vibration of alkyl chains. Aldehyde C–H stretching may be responsible for biosorption/bioaccumulation of As(III) and As(V) onto immobilized bacterial cells as wavenumber shifted from 2852.71318 to 2857.674 cm^{-1} and from 2854.176 to 2847.752 cm^{-1}, respectively. The next biosorption/bioaccumulation peaks at 1658.508 cm^{-1}

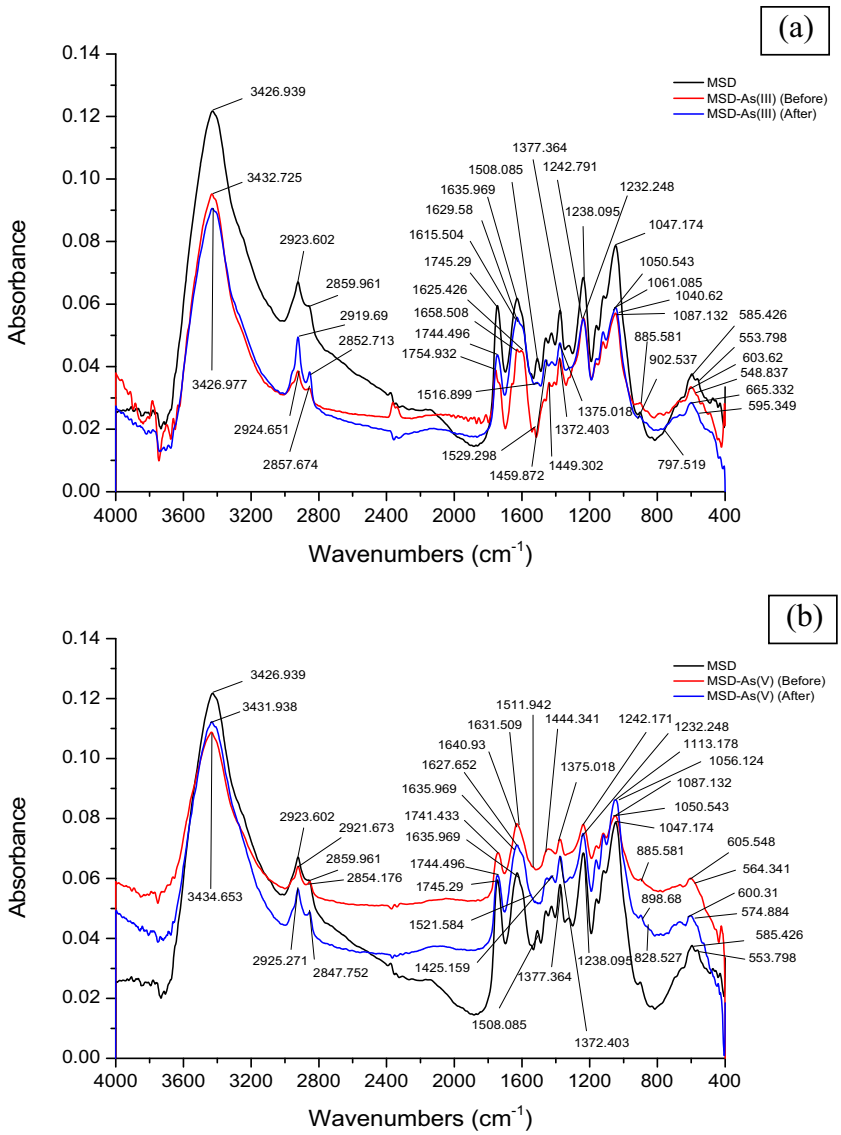

Fig. 1 FT-IR spectra of **a** fresh SD/$MnFe_2O_4$ composite (MSD), As(III) acclimatized *C. glutamicum* MTCC 2745 immobilized on SD/$MnFe_2O_4$ composite before and after As(III) biosorption/bioaccumulation and **b** fresh SD/$MnFe_2O_4$ composite (MSD), As(V) acclimatized *C. glutamicum* MTCC 2745 immobilized on SD/$MnFe_2O_4$ composite before and after As(V) biosorption/bioaccumulation

shifted to 1629.58 cm^{-1} for As(III) and 1640.93023 cm^{-1} shifted to 1635.969 cm^{-1} for As(V), perhaps owing to the complexation of amide group (N–H stretching and C=O stretching vibration) with As(III) and As(V) ions [36]. Another shift was noticed from 1449.30233 to 1459.872 cm^{-1} (As(III)) and from 1444.34109 to 1425.159 cm^{-1} (As(V)), corresponding to the complexation of nitrogen with As(III) and As(V) ions of the N–H group [37, 38]. The peaks at 1087.13178 cm^{-1} (As(III)) and 1087.13178 cm^{-1} As(V) may be attributed to the C–N stretching vibrations of amino groups which shifted to higher frequency and appeared at 1061.085 and 1113.178 cm^{-1}, respectively, owing to the interaction of nitrogen from the amino group with As(III) and As(V) ions [13, 39]. The other weak biosorption/bioaccumulation peak shifted from 885.5814 to 902.5367 cm^{-1} (As(III)) and from 885.5814 to 898.6797 cm^{-1}, corresponding to the O–C–O scissoring vibration of polysaccharide [40, 41]. The band at 603.6196 cm^{-1} (Fig. 1a) and 605.5482 cm^{-1} (Fig. 1b) could be attributed to the existence of Fe–O bond [42, 43], but then it shifted to 665.3315 cm^{-1} after biosorption/bioaccumulation of As(III) (Fig. 1a) and to 600.3101 cm^{-1} after biosorption/bioaccumulation of As(V) (Fig. 1b), respectively. A characteristic peak at 548.83721 cm^{-1} (Fig. 1a) and 564.34109 cm^{-1} (Fig. 1b) could be assigned to Mn–O bond [44, 45] and it had a different variability to 595.3488 cm^{-1} (Fig. 1a) and 574.8837 cm^{-1} (Fig. 1b) for biosorption/bioaccumulation of As(III) and As(V), respectively. The change in wavenumber of Me–O bonds after biosorption/bioaccumulation of As(III) and As(V) specified that both Fe–O and Mn–O bonds were responsible for both $MnFe_2O_4$–As(III) and $MnFe_2O_4$–As(V) [43, 46]. Presence of As(III) and As(V)

on the biosorbent attached with biofilm can be assured from the bands appeared at 797.5194 cm^{-1} (Fig. 1a) and 828.5271 cm^{-1} (Fig. 1b), respectively [47–49]. It has to be cited here that a clear band was very hard to be got in the case of As(III), compared with the distinctive band of As(III) found at 797.5194 cm^{-1} and As(V) found at 828.5271 cm^{-1}. This may be because of different mechanisms involved in As(III) and As(V) biosorption/bioaccumulation. It should be distinguished that the As–O band after biosorption/bioaccumulation of arsenic was not obviously detected owing to the broad overlapping peaks in this region [46].

SEM Analysis

Figure 2a, b exhibited the morphology of As(III) and As(V) acclimatized *C. glutamicum* MTCC 2745 bacterial cells, respectively. From the figure, it is obvious that they were

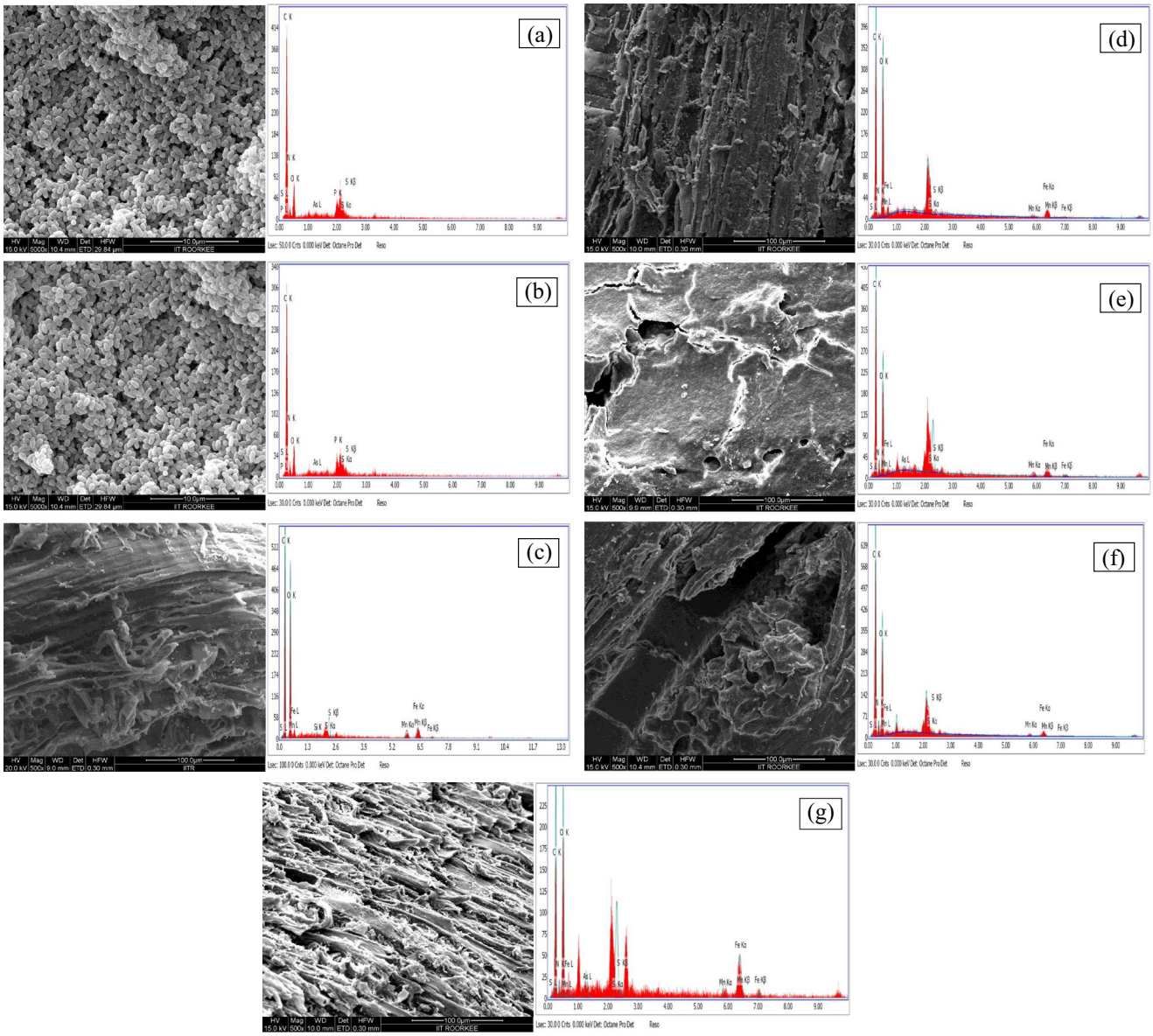

Fig. 2 Scanning electron micrographs (SEM) and EDX of **a** As(III) acclimatized living cells of *C. glutamicum* MTCC 2745 at loaded stage, **b** As(V) acclimatized living cells of *C. glutamicum* MTCC 2745(original magnification, ×5000), **c** fresh SD/$MnFe_2O_4$ composite, **d** As(III) acclimatized *C. glutamicum* MTCC 2745 immobilized on SD/$MnFe_2O_4$ composite at unloaded stage, **e** As(III) acclimatized *C. glutamicum* MTCC 2745 immobilized on NL/$MnFe_2O_4$ composite at loaded stage, **f** As(V) acclimatized *C. glutamicum* MTCC 2745 immobilized on SD/$MnFe_2O_4$ composite at unloaded stage and **g** As(V) acclimatized *C. glutamicum* MTCC 2745 immobilized on SD/$MnFe_2O_4$ composite at loaded stage(original magnification, ×500)

basically rod-like shape. The SEM images of the prepared fresh SD/$MnFe_2O_4$ composite (Fig. 2c) and As(III) acclimatized *C. glutamicum* MTCC 2745 immobilized on surface of SD/$MnFe_2O_4$ composite at stage of unloaded and loaded with As(III) (Fig. 2d, e) and As(V) acclimatized *C. glutamicum* MTCC 2745 immobilized on surface of SD/$MnFe_2O_4$ composite at stage of unloaded and loaded with As(V) (Fig. 2f, g) were also shown. It can be understood from Fig. 2c, manganese ferrite ($MnFe_2O_4$) particles with numerous diameters were arbitrarily distributed onto the acid treated SD surface. It is clear from Fig. 2d, f that most of the active sites of SD/$MnFe_2O_4$ composite were shielded owing to the formation of biofilm on it. The bacterial mass partially occupies the void spaces of the biosorbent surface, so formation of biolayer on the surface of biosorbent decreases its surface porosity [20]. It can be observed from Fig. 2e, g, the immobilized bacterial cells have bulky structure with no porosity. A change in surface morphology from being smooth to rough and occupation of pores specified the As(III) and As(V) biosorption/bioaccumulation on the surface and pores of SD/$MnFe_2O_4$ composite providing it a rough texture (Fig. 2e, g) [50].

The corresponding EDX spectra of the As(III) and As(V) acclimatized bacteria and the unloaded and loaded immobilized bacterial cells were collected and shown in Fig. 2a–g. The presence of iron, manganese and oxygen onto the unloaded composite surface and iron, manganese and oxygen, arsenic on the surface of loaded immobilized bacterial cells were shown clearly. This outcome again recognized the attendance of $MnFe_2O_4$ particles onto the acid treated SD surface in addition to biosorption/bioaccumulation of arsenic onto the surface of immobilized bacterial cells.

Effect of pH

Since both the distribution of arsenic ions in natural water and the overall charge of the biosorbent mainly depends on pH conditions [51, 52], so pH plays a significant governing role in the biosorption/bioaccumulation process to attain maximum arsenic removal by a biosorbent [53]. Therefore, the effect of pH on biosorption/bioaccumulation of As(III) and As(V) by immobilized bacterial cells was investigated by changing the initial pH of the solution in the range of 2.0–12.0 and the results are shown in the Fig. 3. The dependency of uptake of adsorbate on pH is associated to both functional groups on the surface of biosorbents and to chemistry of the adsorbate in aqueous phase. The pH value can change the state of the active-binding sites.

In the pH range of 2.0–9.0 and 10.0–12.0, As(III) occurs mostly in neutral (H_3AsO_3) and anionic ($H_2AsO_3^{-}$) forms, respectively. Reports also confirm that As(V) exists mainly

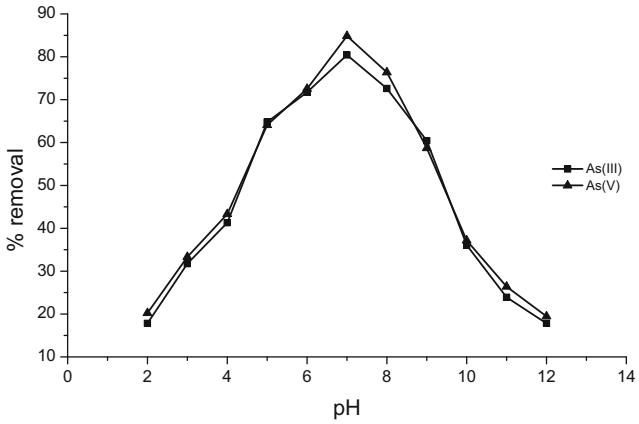

Fig. 3 Effect of pH on As(III) and As(V) removal in SBB studies (C_o: 50 mg/L; T: 30 °C; t: 90 min; M: 4 g/L)

in the monovalent form of $H_2AsO_4^{-}$ in the pH range 3.0–6.0; nevertheless, at pH near 2.0, a small extent of H_3AsO_4 also remains. Whereas a divalent anion $HAsO_4^{2-}$ predominates at higher pH values (>8.0); both species co-exist, in the intermediate region of pH 6.0–8.0 [54]. Arsenic occurs in several oxidation states, and the stability of these ionic species are influenced by the pH of the aqueous system. The speciation of As(III) and As(V) under various pH is shown in Table 4 [55].

It has become evident from Fig. 3 that in the pH range < 3.0, the removal of both As(III) and As(V) ions (31.74 and 33.31 %, respectively) was very poor. With the increase in pH from 3.0 to 7.0, there was a significant increase in removal of both As(III) and As(V) ions. The maximum removal of As(III) and As(V) ions was obtained as 80.435 and 84.846 %, respectively, at pH 7.0. Then, a sharp decline in the removal was observed and As(V) exhibited more removal than As(III). These results can be evident from the following reasons.

The microbe used in the study, i.e. bacteria of *C. glutamicum* MTCC 2745, stops to grow in extreme acidic and extreme alkaline conditions [20, 56]. With the reduction in pH (pH < 7.0), the growth of the bacterial cells reduced, which

Table 4 Stabilities of arsenic species under different pH and redox conditions

Reducing conditions		Oxidizing conditions	
pH	As(III)	pH	As(V)
0–9.0	H_3AsO_3	0–2.0	H_3AsO_4
10.0–12.0	$H_2AsO_3^{-}$	3.0–6.0	$H_2AsO_4^{-}$
13.0	$HAsO_3^{2-}$	7.0–11.0	$HAsO_4^{2-}$
14.0	AsO_3^{3-}	12.0–14.0	AsO_4^{3-}

reduced the % removal of As(III) and As(V). At pH 4.0, the growth of the bacteria was less, as a result the % removal of both As(V) and As(III) was slightly higher than that of the corresponding values acquired by physico-chemical adsorption under the experimental conditions. At pH < 3.0, very less growth of bacteria was observed. With the increase of pH (>7.0), the growth of bacterial cells also decreased. So, the highest removal of As(III) and As(V) ions in biosorption/bioaccumulation process was acquired at pH 7.0.

Moreover, at low pH < 3.0, the density of hydrogen ion was quite high against the As(III) and As(V) ions, which caused the protonation of the components of the cell walls. The protonation of bacterial cell wall moieties affected the biosorption capacity since there was a strong electrostatic interaction remains between positively charged biosorbent surface and oxyanions. Comte et al. established that the deprotonated form of the reactive sites in cell wall, mostly carboxylic, phosphoric and amino groups, is mainly responsible for the binding of metal ions to EPS [57]. It was also shown from FT-IR studies. The solution pH affects the ionization state of these functional groups. Anions could be expected to interact more strongly with cells as the concentration of positive charges rises.

The surface of immobilized bacterial cells are very protonated in extreme acidic conditions and such a condition is not so promising for removal of As(III) due to the presence of neutral As(III) species in this range, causing almost no change in the degree of biosorption/bioaccumulation within the pH range 2.0–5.0. The degree of protonation of the surface declines gradually with the rise in pH of the system. The highest removal of As(III) was at pH 7.0 where only non-ionic species H_3AsO_3 are governing [1], might be attributed to several products of undetermined reaction all through the process of biosorption/bioaccumulation. The neutral (H_3AsO_3) and monoanionic ($H_2AsO_3^-$) species are thus considered to be responsible for the biosorption of As(III), also due to the substitution of hydroxyl ions or water molecules. The neutral species (H_3AsO_3) cannot undergo electrostatic interaction with the biosorbent. However, such species can interact with the unprotonated amino groups [17, 49]. The negative charged $H_2AsO_3^-$ species starts dominant in alkaline medium and thus surface also tends to achieve negative charges (OH^-). This trend of adsorbate species and immobilized bacterial cells will endure to increase with the increase of pH instigating a continuing increase in the repulsive forces between the adsorbate species and immobilized bacterial cells causing in a decrease of biosorption/bioaccumulation [54].

In case of As(V), neutral (H_3AsO_4) and anionic ($H_2AsO_4^-$) species occur at pH 2.0–7.0; however, the prevailing is $H_2AsO_4^-$ [1]. At pH (2.0–7.0), the surface of immobilized bacterial cells is extremely protonated and thus a strong electrostatic interaction remains between positively charged immobilized bacterial cells and oxyanions and as a result the removal improved in this pH range owing to the rise in $H_2AsO_4^-$ species with the pH. The dominant species of As(V) in the above-mentioned pH range are $H_2AsO_4^-$ ions, which can be sorbed on the biosorbent by substituting hydroxyl ions or coordination of hydroxyl groups with the sorbate [17, 58]. Further reduction in removal of As(V) with rise in pH (7.0–12.0) may be clarified as the immobilized bacterial cells may be negatively charged by adsorbing hydroxyl ions onto the surface or by ionization of very weak acidic functional groups of the immobilized bacterial cells or both at higher pH values. A repulsive force may exist between the anionic species and negatively charged surface. This results in reduction of As(V) removal at higher pH values [54].

Mondal et al. estimated the optimum value of pH equivalent to 7.0 in simultaneous adsorption and bioaccumulation study using *Ralstonia eutropha* MTCC 2487 and granular activated carbon and obtained the maximum As(III) and As(V) ions removal about 86 % [20].

Biosorption/Bioaccumulation Mechanism of As(III) and As(V) Ions

The mechanism of any biosorption/bioaccumulation process is a very vital section to understand the characteristics of the material in addition to understand the process, which supports to design a novel biosorbent for forthcoming uses (The details are provided with supplementary materials).

Effect of Biosorbent Dose

Biosorbent dose is also a significant factor which governs the uptake of immobilized bacterial cells for an initial adsorbate concentration. The influence of biosorbent dose on the % removal is shown in Fig. 4. The removal of As(III) and As(V) improved up to 80.453 and 84.846 %, respectively, when the biosorbent dose was increased from 0.1 to 1 g/L. Further increase in biosorbent dose up to 10 g/L had no effect on the removal of arsenic. The increase in biosorbent

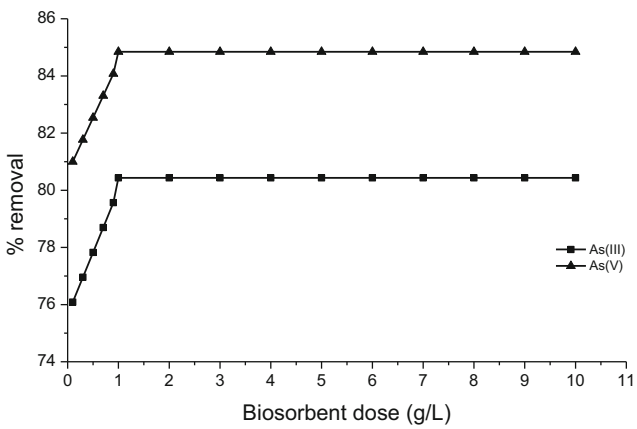

Fig. 4 Effect of SD/$MnFe_2O_4$ composite dose on As(III) and As(V) removal in SBB studies (C_o: 50 mg/L; T: 30 °C; pH: 7.0; t: 90 min)

dose (0.1–1 g/L) resulted in a rapid increase in arsenic ions biosorption/bioaccumulation. This result can be clarified by the statements that during the biosorption/bioaccumulation process, larger surface area was available and the biosorption sites remain unsaturated, while the number of sites available for the biosorption site increases with the increase in the biosorbent dose. With the increase in biosorbent dose, the number of active sites in unit volume of solution increases, which leads to the increase in the % removal of arsenic [47]. On the other hand, with further rise in biosorbent dose (1–10 g/L), there was no prominent difference in the % removal of As(III) and As(V) ions. It may also be owing to the fact that a higher dosage could create a 'screen effect' on the immobilized bacterial cells, protecting the binding sites, therefore the lower arsenic biosorption/bioaccumulation [14]. The decrease in removal efficiency at higher biosorbent dose can also be elucidated as a result of a partial aggregation of immobilized bacterial cells, which results in a reduction in effective surface area for the biosorption/bioaccumulation and overlapping of active sites [59, 60]. So, 1 g/L of SD/$MnFe_2O_4$ composite was selected as the optimum biosorbent dose for further studies.

Effect of Contact Time

Figure 5 shows the influence of contact time on the % removal of As(III) and As(V) using immobilized bacterial cells. Contact time is also a significant factor for the biosorption/bioaccumulation process. From the above observation, it can be concluded that the time compulsory to reach equilibrium for both As(III) and As(V) biosorption/bioaccumulation on immobilized bacterial cells was 240 min. For further rise in time, no notable enhancement was observed in removing arsenic. So, further biosorption/bioaccumulation studies were continued for a contact time of 240 min.

From the consequences, it is further obvious that in all the systems, the saturation time does not depend on the adsorbate concentration in the solution. The change in the rate of removal might be owing to the fact that initially all sites of immobilized bacterial cells are easily accessible and also the concentration gradient of adsorbate is very high. At optimum pH, the fast kinetics of interaction of adsorbate-immobilized bacterial cells might be decided to increase availability of the active sites of the immobilized bacterial cells. So, the removal of adsorbate was fast in the early stages and progressively declines with the interval of time until equilibrium in each case. The reduction in removal of metal ion at the later stage of the process was owing to the lowering of concentration of metal ions [61]. Furthermore, the characteristic of the equilibrium time curve exhibited that the SBB process approaches the equilibrium in short span of time [22]. So, the curves found were single, smooth and continuous leading to equilibrium and suggested the possibility of monolayer coverage of the adsorbate on the immobilized bacterial cells [54].

Effect of Temperature

The temperature has two main influences on biosorption/bioaccumulation process. Temperature essential for the biosorption/bioaccumulation system governs the biosorption/bioaccumulation process as endothermic or exothermic. Increasing the temperature is familiar to raise the rate of diffusion of the adsorbate, due to the reduction in the viscosity of the solution. Besides, changing the temperature will alter the equilibrium biosorption capacity of the immobilized bacterial cells for a specific biosorbent [62].

The effect of temperature on the removal efficiency of As(III) and As(V) was inspected in the range of 20–50 °C during the equilibrium time. The consequences of influence of temperature have been exposed in Fig. 6. It was observed from the Fig. 6 that with a little increase in temperature from 20 to 30 °C, the biosorption/bioaccumulation of arsenic

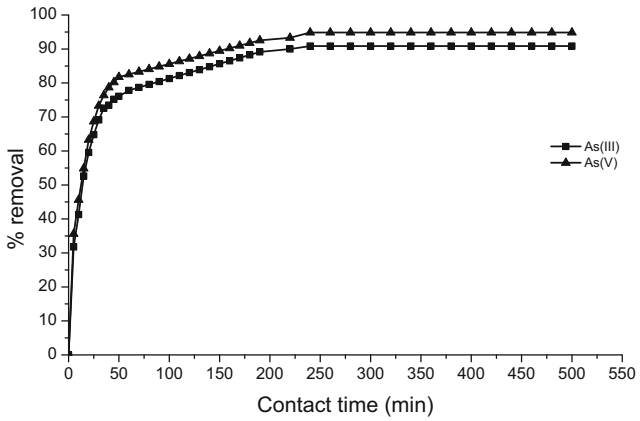

Fig. 5 Effect of contact time on As(III) and As(V) removal in SBB studies (C_o: 50 mg/L; T: 30 °C; pH: 7.0; M: 1 g/L)

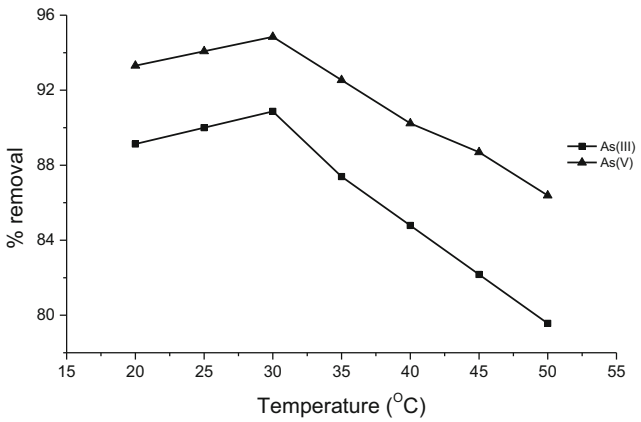

Fig. 6 Effect of temperature on As(III) and As(V) removal in SBB studies (C_o: 50 mg/L; pH: 7.0; M: 1 g/L; t: 240 min)

(As(III) or As(V)) ions on immobilized bacterial cell surface increased. After 30 °C temperature, the removal of arsenic (As(III) or As(V)) ions by immobilized bacterial cell decreased with the increase in temperature. For As(III) and As(V), % removal decreased from 90.87 to 79.565 % and 94.846 to 86.385 %, respectively, with increase in temperature from 30 to 50 °C.

The favourable temperature for the growth of *C. glutamicum* MTCC 2745 is 30 °C according to the guideline of MTCC. The result specified that the highest removal was got at a temperature of 30 °C in biosorption/bioaccumulation system. Further rise in temperature resulted in lower scavenging efficiency for arsenic removal in biosorption/bioaccumulation system.

This can also be clarified by the exothermicity of the biosorption/bioaccumulation process. Temperature influences the interaction between the biomass and the metal ions, generally by impacting the stability of the metal-sorbent complex and the ionization of the cell wall moieties [63]. The temperature of the biosorption solution could be vital for energy dependent mechanisms in metal binding process [64]. Energy independent mechanisms are less expected to be influenced by temperature because the processes responsible for biosorption are mainly physico-chemical in nature [65, 66]. The results acquired in the current study indicated that the metal ion sorption in SBB system was exothermic. Kacar et al. [65] and Ozdemir et al. [66] reported in their work about the exothermic behaviour of metal ion sorption on the bacterial surface. The authors correlated their research outcomes as an energy independent mediated sorption of metal ions.

This can also be clarified by the spontaneity of the biosorption/bioaccumulation process. Initial rise in removal efficiency up to 30 °C is mainly because of the rise in collision frequency between biosorbent and adsorbate. Further rise in temperature (>30 °C) caused lower removal efficiency for arsenic removal by immobilized bacterial cells. This reduction in scavenging efficiency might be owing to many factors: the relative increase in the dodging tendency of the arsenic ions from the solid biosorbent phase to the bulk liquid phase; deactivating immobilized bacterial cells or destructing some active sites on the surface of immobilized bacterial cells due to bond ruptures [67, 68] or owing to the weakening of biosorptive forces between the adsorbate species and the active sites of the immobilized bacterial cells and also between the adjacent molecules of adsorbed phase for high temperatures or movement of biosorbents with more speed, so, lower interaction time with the biosorbent active sites was available for them [69, 70].

Effect of Initial Arsenic Concentration

Effect of initial metal ion concentration on the % removal of arsenic in biosorption/bioaccumulation system is presented in Fig. 7. All the parameters, such as pH, biosorbent dose, contact time and temperature, remain constant; it can be safely concluded that positive and the negative charge density on the surface of immobilized bacterial cells at the initial stages of biosorption/bioaccumulation must have remained constant.

With rise in initial arsenic concentrations, more arsenic ions are left un-adsorbed in the solution owing to the saturation of the binding sites. This recognizes that energetically less favourable binding sites become involved with rising ions concentration in aqueous solution. Removal process of arsenic ions is referred to various ion exchange mechanisms along with the biosorption/bioaccumulation process. Throughout the ion exchange process, the arsenic ions have to be transferred through the biosorbent pores, but also through the lattice channel, they have to be substituted exchangeable anions. Diffusion was quicker through pores and was arrested when the ion transfers through the channels with smaller diameter. Here, the biosorption/bioaccumulation of arsenic ion is typically attributed to ion exchange reactions in the biosorbents micro pores [71].

Effect of initial metal ion concentration in terms of distribution coefficient R_d, as defined in Eq. 5, is presented in Fig. 8. The distribution coefficient (R_d) can be used as a significant tool to estimate mobility of metal ion. The R_d values reduced with the rising concentration of adsorbate. High values of distribution coefficient, R_d, indicated that the adsorbate has been engaged by the biosorbent attached with biofilm through biosorption/bioaccumulation process, whereas low values of R_d indicated that a large portion of the adsorbate leftovers in solution [53]. With the increase in concentration of As(III) and As(V), a corresponding decrease in the R_d value from 9.952 to 1.775 L/g and from 18.403 to 2.189 L/g, respectively, suggested the fixed number of biosorption sites obtainable for biosorption/bioaccumulation. This effect can also be clarified as at high

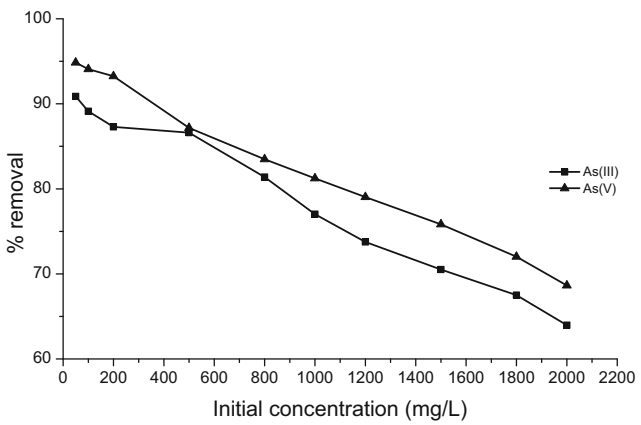

Fig. 7 Effect of initial arsenic concentration on As(III) and As(V) removal in SBB studies (pH: 7.0;M: 1 g/L; t: 240 min; T: 30 °C)

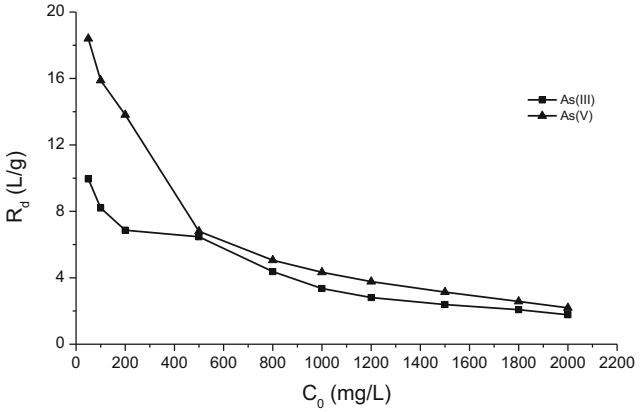

Fig. 8 Distribution coefficient (R_d) of As(III) and As(V) biosorbed on *C. glutamicum* MTCC 2745 immobilized on surface of SD/$MnFe_2O_4$ composite

adsorbate/biosorbent attached with biofilm ratios, biosorption/bioaccumulation of adsorbate contains higher energy sites. As the adsorbate/biosorbent attached with biofilm ratio rises, the higher energy sites are saturated and biosorption initiates on lower energy sites, affecting in decreases in the % removal of adsorbate [71]. These results repeat the efficiency of biosorbent material attached with biofilm for the elimination of arsenic from liquid phase over a broad range of concentrations in biosorption/bioaccumulation system.

Model Selection: Error Analysis and Maximum Adsorption Capacity

The optimum parameter sets, evaluated on the basis of higher correlation coefficient (R, R^2 and $\overline{R^2}$) and lower error values (SSE, Reduced χ^2 and Root–MSE), were estimated by considering 95 % confidence interval. The ideal parameters along with the correlation coefficients and error values are given in the Tables 5, 6 and 7.

One-Parameter Model

Henry's law was unsuccessful for defining the experimental data obtained for the biosorption/bioaccumulation of arsenic (As(III) and As(V)) on immobilized bacterial cells (Fig. 9a, b). The highest error values (SSE, Reduced χ^2 and Root–MSE) and the lowest correlation coefficient values (R, R^2 and $\overline{R^2}$) for both As(III) and As(V) indicated that this model is really ineffective to predict the equilibrium data (Table 5). It might be because of the non-availability of biosorption/bioaccumulation data in the vanishing range of arsenic. Generally, in liquid phase biosorption/bioaccumulation, the equilibrium data are attained at higher equilibrium adsorbate concentrations, while the immobilized bacterial cells are almost at the edge of saturation. Therefore, this research established the fact of let-down of Henry's law at the high ranges of residual adsorbate concentration.

Two-Parameter Model

Among all the other two-parameter models (Fig. 9a, b), the Langmuir isotherm showed a good fit to the experimental data for both As(III) and As(V) due to the highest correlation coefficient (R, R^2 and $\overline{R^2}$) and the lowest error values (SSE, Reduced χ^2 and Root–MSE) (Table 5) and a high q_{mL} value. This recognized the homogeneous and monolayer manner of biosorption/bioaccumulation of As(III) and As(V) on immobilized bacterial cells. Also, it delivered provision to the supposition that biosorption/bioaccumulation of As(III) and As(V) happened uniformly on the active sites of the immobilized bacterial cells, and once a molecule occupies a site, no more biosorption/bioaccumulation could happen at this site. The separation factor (R_L) value (Fig. 10) which is a measure of biosorption/bioaccumulation favourability assessed from the Langmuir isotherm recognized that As(III) and As(V) biosorption/bioaccumulation on the surface of immobilized bacterial cells were in favourable region ($0 < R_L < 1$). The reduction in R_L with a rise in the initial concentration has accepted that the biosorption/bioaccumulation was more encouraging at high concentrations.

On the other hand, the acquired error values and correlation coefficient values in case of Jovanovic model acknowledged better fit with the experimental data for As(III) and As(V), respectively, to some extent though having lower maximum adsorption capacity than Langmuir isotherm.

Also, Freundlich isotherm (Table 5) closely fitted to the equilibrium data in providing of the suppositions of heterogeneous manner of biosorption/bioaccumulation to a certain extent because of high correlation coefficient and low error values. But Freundlich isotherm model fit as well as Langmuir and Jovanovic isotherm. The respective value of n_F of Freundlich isotherm, 1.95502 and 1.99542 for As(III) and As(V), respectively, showed that the biosorption/bioaccumulation of both As(III) and As(V) on the surface of immobilized bacterial cells was favourable biosorption/bioaccumulation.

The attained high correlation coefficient and low error values of activated sludge isotherm model established the better fit of equilibrium data as compared with Temkin and Dubinin–Radushkevich isotherm models. Though, activated sludge isotherm model was not as good as Langmuir, Freundlich and Jovanovic isotherm. A low value of K_m, 20.26035 and 25.44612 for As(III) and As(V), respectively, activated sludge isotherm recommended that the tendency of formation of floc was probable but little. A lower value of 1/N_m (<1) attained from activated sludge isotherm evaluated that any huge change in the equilibrium arsenic concentration

Table 5 Isotherm constants of one-parameter and two-parameter models for As(III) and As(V) biosorption/bioaccumulation on *C. glutamicum* MTCC 2745 immobilized on surface of SD/$MnFe_2O_4$ composite

Isotherm models	Parameters	Values for As(III)	Values for As(V)
Henry	K_{HE} (L/g)	2.173	2.712
	Reduced χ^2	41789.969	49335.291
	SSE	417899.692	493352.910
	R	0.905	0.902
	R^2	0.818	0.814
	$\overline{R^2}$	0.818	0.814
	Root–MSE	204.426	222.115
Langmuir	q_{mL} (mg/g)	1672.322	1861.715
	K_L (L/mg)	0.004	0.004
	Reduced χ^2	1544.280	1393.368
	SSE	13898.518	12540.311
	R	0.997	0.998
	R^2	0.994	0.995
	$\overline{R^2}$	0.993	0.995
	Root–MSE	39.297	37.328
Freundlich	K_F ((mg/g)(L/mg)$^{1/nF}$)	46.151	57.017
	n_F	1.955	1.995
	Reduced χ^2	2312.077	1514.244
	SSE	20808.694	13628.193
	R	0.995	0.997
	R^2	0.991	0.995
	$\overline{R^2}$	0.990	0.994
	Root–MSE	48.084	38.913
Temkin	b_{TE} (J/mol)	9.940	10.318
	K_{TE} (L/mg)	0.128	0.223
	Reduced χ^2	12651.487	19481.860
	SSE	113863.379	175336.743
	R	0.975	0.966
	R^2	0.950	0.934
	$\overline{R^2}$	0.945	0.926
	Root–MSE	112.479	139.577
Dubinin–Radushkevich	q_{mDR} (mg/g)	1134.766	1289.676
	K_{DR} (mol^2/KJ^2)	0.002	0.002
	E (KJ/mol)	15.811	15.811
	Reduced χ^2	27222.822	25371.326
	SSE	245005.394	228341.937
	R	0.945	0.956
	R^2	0.893	0.914
	$\overline{R^2}$	0.882	0.904
	Root–MSE	164.993	159.284
Activated Sludge	K_m (L/g)	20.260	25.446
	N_m	1.955	1.995
	Reduced χ^2	2312.077	1514.245
	SSE	20808.697	13628.209
	R	0.995	0.997
	R^2	0.991	0.995
	$\overline{R^2}$	0.990	0.994
	Root–MSE	48.084	38.913
Jovanovic	q_{mJV} (mg/g)	1291.900	1417.420
	K_{JV} (L/g)	0.004	0.005
	Reduced χ^2	3141.767	2379.943
	SSE	28275.901	21419.490
	R	0.994	0.996
	R^2	0.988	0.992
	$\overline{R^2}$	0.986	0.991
	Root–MSE	56.051	48.785

would not result in a visible change in the amount of formation of floc of arsenic by immobilized bacterial cells.

Temkin and Dubinin–Radushkevich isotherm models did not fit well with the experimental data due to low correlation coefficients and high error values than that for Langmuir isotherm model (Table 5) specified that the mechanism of biosorption/bioaccumulation did not carry on either with progressive widening of biosorbent surfaces or heterogeneous biosorption manner in total (Fig. 9a, b). The mean free energy of adsorption, E estimated from Dubinin–Radushkevich were 15.81139 KJ/mol for both As(III) and As(V), was signifying that the biosorption/bioaccumulation of As(III) and As(V) using by immobilized bacterial cells happened through ion exchange mechanism. The larger value of b_{TE} for both As(III) and As(V) (9.93981 KJ/mol and 10.31756 KJ/mol for As(III) and As(V), respectively) achieved from Temkin isotherm specified that the interaction between As(III) or As(V) and immobilized bacterial cells was strong and the positive value of b_{TE} specified an exothermic process. So, the biosorption/bioaccumulation process of As(III) and As(V) on immobilized bacterial cells can be taken as chemisorption mechanism, as specified by the value of b_{TE}.

Three-Parameter Model

The abilities of the three-parameter equations for modelling the equilibrium biosorption/bioaccumulation data were verified using non-linear regression analysis, and their isotherm parameters are shown in Fig 11a, b and Table 6. All the models appropriately simulated the adsorption isotherms of the studied systems, and the equilibrium As(III) and As(V) uptake by immobilized

Table 6 Isotherm constants of three-parameter models for As(III) and As(V) biosorption/bioaccumulation on *C. glutamicum* MTCC 2745 immobilized on surface of SD/$MnFe_2O_4$ composite

Isotherm models	Parameters	Values for As(III)	Values for As(V)
Redlich–Peterson	K_{RP} (L/g)	11.988	19.579
	α_{RP} $(L/mg)^{\beta}$	0.049	0.111
	β_{RP}	0.723	0.659
	Reduced χ^2	570.872	460.879
	SSE	4566.980	3687.029
	R	0.999	0.999
	R^2	0.998	0.999
	$\overline{R^2}$	0.998	0.998
	Root–MSE	23.893	21.468
Sips	q_{mS} (mg/g)	2300.348	2837.013
	K_S $(m/Lg)^{-1/ms}$	0.008	0.009
	m_S	0.770	0.719
	Reduced χ^2	783.906	232.792
	SSE	6271.251	1862.340
	R	0.999	1.000
	R^2	0.997	0.999
	$\overline{R^2}$	0.997	0.999
	Root–MSE	27.998	15.258
Toth	K_T (L/mg)	0.004	0.005
	q_{mT} (mg/g)	2310.960	2845.265
	m_T	0.647	0.580
	Reduced χ^2	809.172	585.324
	SSE	6473.372	4682.595
	R	0.999	0.999
	R^2	0.997	0.998
	$\overline{R^2}$	0.996	0.998
	Root–MSE	28.446	24.193
Brouers–Sotolongo	q_{mBS} (mg/g)	1687.782	1908.550
	K_{BS} $((mg/g)(L/mg)^{1/\alpha})$	0.013	0.015
	α	0.718	0.698
	Reduced χ^2	882.997	179.148
	SSE	7063.975	1433.185
	R	0.998	1.000
	R^2	0.997	0.999
	$\overline{R^2}$	0.996	0.999
	Root–MSE	29.715	13.385
Vieth–Sladek	K_{VS} (L/mg)	0.709	0.788
	q_{mVS} (mg/g)	901.051	1058.640
	β_{VS}	0.010	0.010
	Reduced χ^2	475.099	999.591
	SSE	3800.790	7996.730
	R	0.999	0.998
	R^2	0.998	0.997
	$\overline{R^2}$	0.998	0.996
	Root–MSE	21.797	31.616
Koble–Corrigan		6.892	8.122
	B_{KC} $(L/g)^{nKC}$	0.004	0.004
	n_{KC}	1.000	1.000
	Reduced χ^2	1737.358	1567.578
	SSE	13898.864	12540.625
	R	0.997	0.998
	R^2	0.994	0.995
	$\overline{R^2}$	0.992	0.994
	Root–MSE	41.682	39.593
Khan	q_{mK} (mg/g)	512.729	359.888
	b_K (L/mg)	0.020	0.045
	a_K	0.639	0.584
	Reduced χ^2	504.028	599.473
	SSE	4032.226	4795.786
	R	0.999	0.999
	R^2	0.998	0.998
	$\overline{R^2}$	0.998	0.998
	Root–MSE	22.451	24.484
Hill	n_H	0.770	0.719
	K_H (L/g)	125.854	106.271
	q_{mH} (mg/g)	2300.005	2837.100
	Reduced χ^2	783.907	232.793
	SSE	6271.255	1862.341
	R	0.999	1.000
	R^2	0.997	0.999
	$\overline{R^2}$	0.997	0.999
	Root–MSE	27.998	15.258
Jossens	K_J ((mg/g)(L/mg))	11.988	19.569
	J $(L/mg)^{bJ}$	0.049	0.111
	b_J	0.723	0.659
	Reduced χ^2	570.872	460.877
	SSE	4566.978	3687.018
	R	0.999	0.999
	R^2	0.998	0.999
	$\overline{R^2}$	0.998	0.998
	Root–MSE	23.893	21.468
Fritz–Schlunder–III	K_{FS} $(L/mg)^{nFS}$	0.049	0.111
	q_{mFS} (mg/g)	244.733	175.645
	m_{FSI}	0.723	0.659
	Reduced χ^2	570.873	460.879
	SSE	4566.981	3687.029
	R	0.999	0.999
	R^2	0.998	0.999
	$\overline{R^2}$	0.998	0.998

Table 6 (continued)

Isotherm models	Parameters	Values for As(III)	Values for As(V)
	$\overline{R^2}$		
	Root–MSE	23.893	21.468
Unilan	q_{mU} (mg/g)	1776.581	1978.622
	s	1.000	1.000
	K_U (L/mg)	0.004	0.004
	Reduced χ^2	1334.848	1275.086
	SSE	10678.781	10200.689
	R	0.998	0.998
	R^2	0.995	0.996
	$\overline{R^2}$	0.994	0.995
	Root–MSE	36.536	35.708
Holl–Krich	q_{mHK} (mg/g)	2300.471	2837.011
	K_{HK} (L/mg)^{nHK}	0.008	0.009
	n_{HK}	0.770	0.719
	Reduced χ^2	783.906	232.792
	SSE	6271.250	1862.340
	R	0.999	1.000
	R^2	0.997	0.999
	$\overline{R^2}$	0.997	0.999
	Root–MSE	27.998	15.258
Langmuir–Freundlich	q_{mLF} (mg/g)	2302.431	2835.278
	K_{LF} (L/mg)	0.002	0.002
	m_{LF}	0.769	0.719
	Reduced χ^2	783.908	232.793
	SSE	6271.262	1862.343
	R	0.999	1.000
	R^2	0.997	0.999
	$\overline{R^2}$	0.997	0.999
	Root–MSE	27.998	15.258
Langmuir–Jovanovic	q_{mLJ} (mg/g)	1755.177	2043.418
	K_{LJ} (L/mg)	0.014	0.016
	n_{LJ}	0.692	0.662
	Reduced χ^2	789.817	225.456
	SSE	6318.535	1803.648
	R	0.999	1.000
	R^2	0.997	0.999
	$\overline{R^2}$	0.997	0.999
	Root–MSE	28.104	15.015
Jovanovic–Freundlich	q_{mJF} (mg/g)	1688.491	1907.898
	n	0.718	0.698
	K_{JF} (L/mg)	0.002	0.002
	Reduced χ^2	882.999	179.149
	SSE	7063.992	1433.188
	R	0.998	1.000
	R^2	0.997	0.999

Table 6 (continued)

Isotherm models	Parameters	Values for As(III)	Values for As(V)
	$\overline{R^2}$	0.996	0.999
	Root–MSE	29.715	13.385
Radke–Prausnitz I	K_{RPI} (L/mg)	0.020	0.045
	q_{mRPI} (mg/g)	512.729	359.888
	m_{RPI}	0.639	0.584
	Reduced χ^2	504.028	599.473
	SSE	4032.226	4795.786
	R	0.999	0.999
	R^2	0.998	0.998
	$\overline{R^2}$	0.998	0.998
	Root–MSE	22.451	24.484
Radke–Prausnitz II	q_{mRPII} (mg/g)	244.733	175.645
	K_{mRPII} (L/mg)	0.049	0.111
	m_{RPII}	0.723	0.659
	Reduced χ^2	570.873	460.879
	SSE	4566.981	3687.029
	R	0.999	0.999
	R^2	0.998	0.999
	$\overline{R^2}$	0.998	0.998
	Root–MSE	23.893	21.468
Radke–Prausnitz III	q_{mRPIII} (mg/g)	12.002	19.512
	K_{RPIII} (L/mg)	20.337	9.042
	m_{RPIII}	0.277	0.341
	Reduced χ^2	570.872	460.877
	SSE	4566.973	3687.017
	R	0.999	0.999
	R^2	0.998	0.999
	$\overline{R^2}$	0.998	0.998
	Root–MSE	23.893	21.468
Langmuir–Freundlich–Jovanovic	q_{mLFJ} (mg/g)	1807.519	2126.619
	n_{LFJ}	0.669	0.635
	K_{LFJ} (L/mg)	0.002	0.002
	Reduced χ^2	763.740	244.977
	SSE	6109.923	1959.814
	R	0.999	1.000
	R^2	0.997	0.999
	$\overline{R^2}$	0.997	0.999
	Root–MSE	27.636	15.652

bacterial cells were sincerely well signified with good correlation coefficient values (R, R^2 and $\overline{R^2}$) and low error values (SSE, Reduced χ^2 and Root–MSE). The appropriateness of these isotherms again confirmed the homogeneous biosorption/bioaccumulation on the

Table 7 Isotherm constants of four-parameter and five-parameter models for As(III) and As(V) biosorption/bioaccumulation on *C. glutamicum* MTCC 2745 immobilized on surface of SD/$MnFe_2O_4$ composite

Isotherm models	Parameters	Values for As(III)	Values for As(V)
Marczewski–Jaroniec	q_{mMJ} (mg/g)	2305.486	2839.466
	K_{MJ} (L/mg)	0.002	0.001
	n_{MJ}	0.751	0.725
	m_{MJ}	0.795	0.711
	Reduced χ^2	892.179	263.813
	SSE	6245.251	1846.688
	R	0.999	1.000
	R^2	0.997	0.999
	$\overline{R^2}$	0.996	0.999
	Root–MSE	29.869	16.242
Baudu	q_{mB} (mg/g)	2300.938	2836.590
	x	−0.231	−0.281
	y	1.000	1.000
	$_{bB}$ (L/mg)	0.008	0.009
	Reduced χ^2	895.893	266.048
	SSE	6271.248	1862.339
	R	0.999	1.000
	R^2	0.997	0.999
	$\overline{R^2}$	0.996	0.999
	Root–MSE	29.931	16.311
Fritz–Schlunder–IV	A_{FS} ((mg/g)(L/mg)^{aFS})	11.960	28.256
	B_{FS} (L/mg)^{bFS}	0.049	0.003
	a_{FS}	1.000	0.685
	b_{FS}	0.724	0.841
	Reduced χ^2	682.197	211.734
	SSE	4775.382	1482.140
	R	0.999	1.000
	R^2	0.998	0.999
	$\overline{R^2}$	0.997	0.999
	Root–MSE	26.119	14.551
Fritz–Schlunder–V	q_{mFSS} (mg/g)	11.984	30.097
	K_1 (L/mg)$^{\alpha FS}$	1.000	1.000
	K_2 (L/mg)$^{\beta FS}$	0.049	0.001
	α_{FS}	1.000	0.658
	β_{FS}	0.723	1.000
	Reduced χ^2	761.512	192.958
	SSE	4569.072	1157.750
	R	0.999	1.000
	R^2	0.998	1.000
	$\overline{R^2}$	0.997	0.999
	Root–MSE	27.596	13.891

heterogeneous surface of immobilized bacterial cells and the cooperative manifestations of the biosorptive As(III) and As(V) ions.

In case of As(III) on the basis of the maximum correlation coefficients (R, R^2 and $\overline{R^2}$) and the lowest error values (SSE, Reduced χ^2 and Root–MSE), the better and perfect illustration of the experimental outcomes was attained using Vieth–Sladek isotherm among the verified three-parameter isotherm (Fig. 11a, b). Vieth–Sladek isotherm constant, K_{VS}, was closely equal to zero revealed that the biosorption data trailed the suppositions of Langmuir isotherm.

The value of Vieth–Sladek isotherm constant, K_{VS}, was nearly equal to zero showed that the biosorption data trailed the assumptions of Langmuir isotherm. The value of Vieth–Sladek model exponent β_{VS} for As(V) tending to zero indicated that the data can desirably fit with Langmuir model. This is ascertained by the suitable fit of the data to Langmuir model. Vieth–Sladek isotherm is utilized for calculating diffusion rates in solid materials from transient adsorption. Especially, this isotherm applies to adsorbates which are adsorbed according to a specific isotherm: one defined by a linear component (Henry's law) and a commonly found non-linear component (Langmuir equation). The linear component relates physically to gas dissolved in the amorphous regions and, the non-linear, to the adherence of gas molecules to sites on the surface of porous adsorbents [72].

However, for As(V), based on maximum correlation coefficients (R, R^2 and $\overline{R^2}$) and the lowest error values (SSE, Reduced χ^2 and Root–MSE), the greater and perfect demonstration of the experimental results was observed using Brouers–Sotolongo isotherm model (Fig. 11a, b) among all the tested isotherm models.

Brouers–Sotolongo isotherm was competent to describe the biosorption/bioaccumulation process taken into consideration from the beginning that it is a complex system. Certainly immobilized bacterial cells has strong heterogeneous surface that stems from two sources recognized as geometrical and chemical ones [73]. Geometrical heterogeneity is mostly a result of variances in size and shape of pores, cracks and pits. Chemical heterogeneity is connected to numerous functional groups, e.g. phenols, carbonyls, aldehydes, lactones of surface of immobilized bacterial cells. Both geometrical and chemical heterogeneities add strongly to the biosorption/bioaccumulation of As(III) and As(V) on the surface of immobilized bacterial cells [74].

The maximum adsorption capacity predicted by Sips, Toth, Brouers–Sotolongo, Hill, Unilan, Holl–Krich, Langmuir–Freundlich, Langmuir–Jovanovic, Jovanvic–Freundlich and Langmuir–Freundlich–Jovanovic was higher than Langmuir isotherm but it was observed

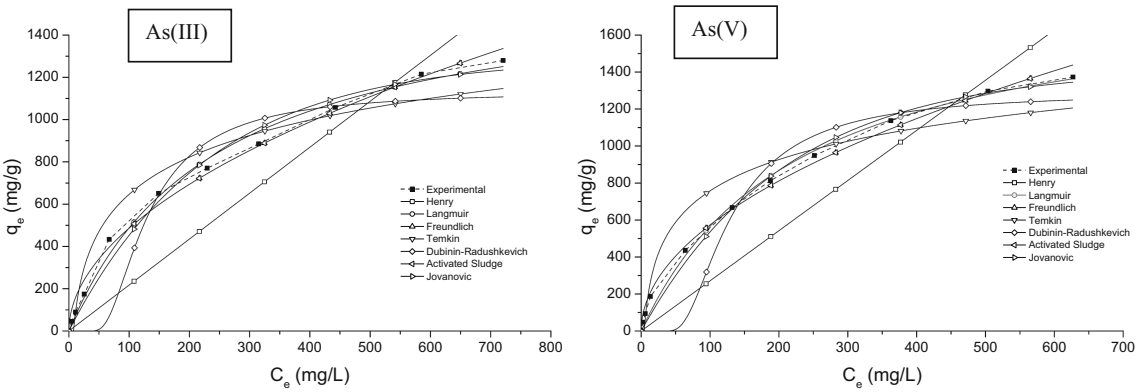

Fig. 9 Isotherm modelling of As(III) and As(V) biosorption/bioaccumulation on *C. glutamicum* MTCC 2745 immobilized on surface of SD/$MnFe_2O_4$ composite for one and two-parameter models (C_o: 50–2000 mg/L; M: 1 g/L; pH: 7.0; t: 240 min; T: 30 °C)

opposite in the case of Vieth–Sladek, Khan, Fritz–Schlunder–III, Radke–Prausnitz I, II and III isotherms for both As(III) and As(V).

The values of β_{RP}, m_S, m_T, a_K, m_{FSI}, m_{LF}, n_{LJ}, m_{RPI}, m_{RPII} and n_{LFJ} for both As(III) and As(V) approaching unity specified that the biosorption/bioaccumulation data observed in this study were more of a Langmuir form rather than that of Freundlich isotherm.

The values of m_{RPIII} for both As(III) and As(V) were observed to be close to zero which indicated that the model supported Langmuir model. The Hill model exponent n_H for both As(III) and As(V) were <1, conveyed the fact that the binding interaction between As(III) or As(V) and immobilized bacterial cells was in the form of negative cooperativity.

Though the correlation coefficient values were moderately good for all the three-parameter models (Table 6), poor error values (SSE, Reduced χ^2 and Root–MSE) clearly indicated that Koble–Corrigan and Unilan isotherm were unsuccessful to fit the experimental equilibrium data may be due to the fact that the most of the active sites might have adsorption energy higher than maximum value.

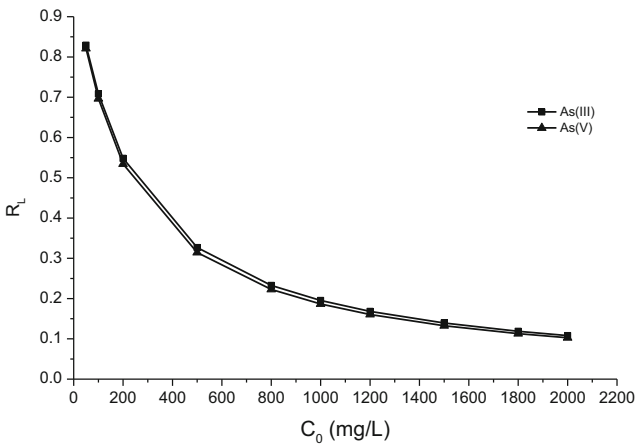

Fig. 10 Plot of separation factor (R_L) versus initial As(III) and As(V) concentration

Four-Parameter Model

Among three isotherms of four-parameter models (Fig. 12a, b; Table 7), very well fitting of the experimental results of biosorption/bioaccumulation data for both As(III) and As(V) were found using Fritz–Schlunder–IV isotherm with the lowest error values and the highest correlation coefficient values for both As(III) and As(V)). This isotherm was found to be slightly better than Marczewski–Jaroniec and Baudu isotherm models on the basis of correlation coefficient (R, R^2 and $\overline{R^2}$) and error values (SSE, reduced χ^2 and Root–MSE).

Furthermore, the values of a_{FS} and b_{FS} for both As(III) and As(V) approaching unity stated that the biosorption/bioaccumulation data can suitably be fitted with the Langmuir isotherm. The parameters assessed A_{FS} and B_{FS}, and a value of A_{FS}/B_{FS} was revealing the adsorbate and adsorbent interaction strength. Similarity was also observed between the B_{FS} and the Langmuir constant K_L.

Also, the values of n_{MJ} and m_{MJ} for As(III) approaching unity stated that the biosorption/bioaccumulation data can preferably be fitted with the Langmuir isotherm. Wherever in case of As(V), the values of n_{MJ} and m_{MJ} also approaching unity indicated that the biosorption/bioaccumulation data can also preferably be fitted with the Langmuir isotherm. Similarity has also been observed between the K_{MJ} and the Langmuir constant K_L.

Fritz–Schlunder–IV and Baudu isotherms yet again confirmed the fact that the biosorption/bioaccumulation of As(III) and As(V) on the surface of immobilized bacterial cells was homogeneous and characteristically followed Langmuir isotherm; however, the biosorption/bioaccumulation was happening on the heterogeneous surface.

Five-Parameter Isotherm

The biosorption/bioaccumulation data were analyzed in keeping with the non-linear form of the five-parameter

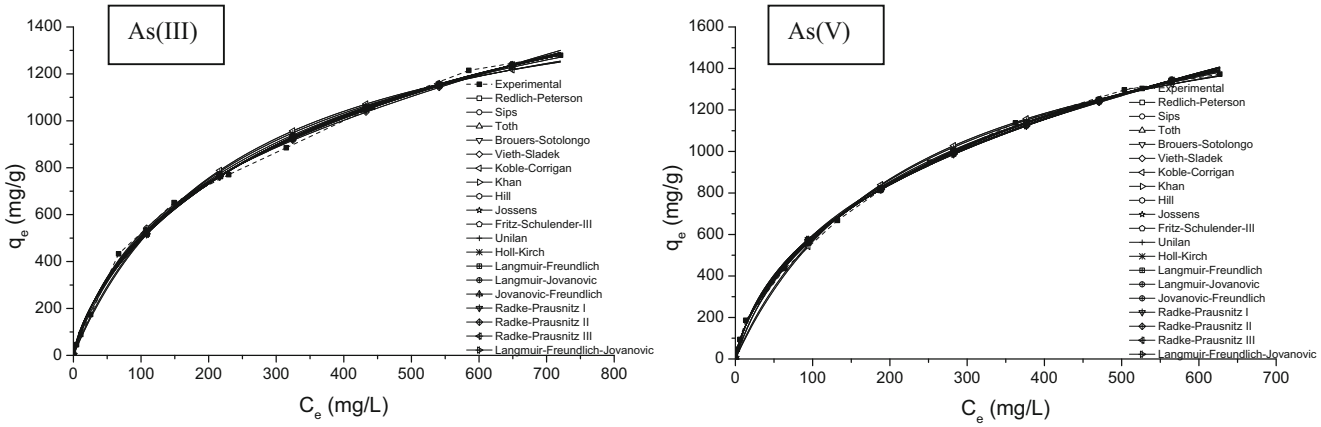

Fig. 11 Isotherm modelling of As(III) and As(V) biosorption/bioaccumulation on *C. glutamicum* MTCC 2745 immobilized on surface of SD/$MnFe_2O_4$ composite for three-parameter models (C_o: 50–2000 mg/L; M: 1 g/L; pH: 7.0; t: 240 min; T: 30 °C)

isotherm model of Fritz–Schlunder–V. A proper fitting of the experimental data of the adsorption isotherms achieved employing the five-parameter model of Fritz–Schlunder–V (Fig. 12a, b; Table 7) with the lowest error values (SSE, reduced χ^2 and Root–MSE) and the highest correlation coefficient values (R, R^2 and $\overline{R^2}$) for both As(III) and As(V) was found. The values of α_{FS} and β_{FS} for both As(III) and As(V) were very close to unity which showed that the biosorption/bioaccumulation data followed the suppositions of Langmuir isotherm.

Final Remarks on Isotherm Study

The experimental equilibrium data are observed to be well fitted with the Langmuir isotherm model among two-parameter isotherm models which stated the monomolecular biosorption/bioaccumulation of As(III) and As(V) on the surface of immobilized bacterial cells. The value of correlation coefficient (R, R^2 and $\overline{R^2}$) and error values (SSE, reduced χ^2 and Root–MSE) showed the best fit to the adsorption isotherm data of As(III) among all the models using Vieth–Sladek isotherm model. Vieth–Sladek model exponent recommended that the biosorption/bioaccumulation data got in this study was more of Langmuir form rather than that of Freundlich isotherm and the current data supported monolayer mode of biosorption. It was well-fitting Brouers–Sotolongo isotherm model among three-parameter isotherm models for As(V) and its model exponent recommended that this isotherm is proficient to define the biosorption process happening from the beginning is a complex system. Among four-parameter isotherm models, most well-fitting isotherm was Fritz–Schlunder–IV isotherm for both As(III) and As(V) and similarity was also found between the B_{FS} and the Langmuir constant K_L.

The adjusted coefficient of determination ($\overline{R^2}$), which generally accounts for the number of variables and sample size in the model, is considered superior to the coefficient of determination (R^2), as it revises the overestimation by R^2 [75]. It is more exact than R^2 specially when dealing with small samples.

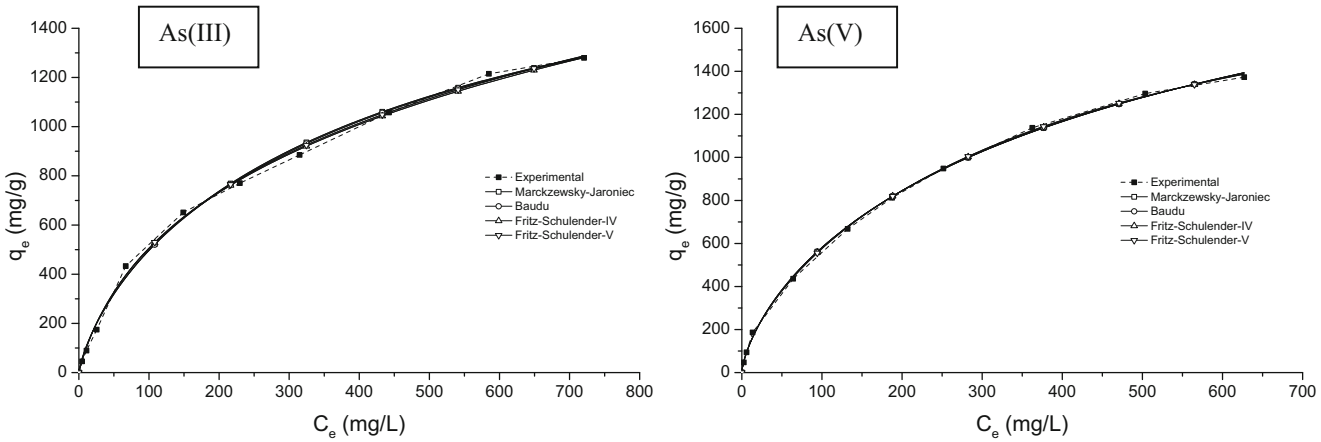

Fig. 12 Isotherm modelling of As(III) and As(V) biosorption/bioaccumulation on *C. glutamicum* MTCC 2745 immobilized on surface of SD/$MnFe_2O_4$ composite for four and five-parameter models (C_o: 50–2000 mg/L; M: 1 g/L; pH: 7.0; t: 240 min; T: 30 °C)

On the basis of $\overline{R^2}$ values, the higher fitted model order among one and two-parameter models in decreasing manner is shown in Table S4 of supplementary materials. Based on $\overline{R^2}$ values, the best fitted model order among one and two-parameter models was Langmuir model with a maximum adsorption capacity of 1672.32214 mg/g for As(III) and 1861.71453 mg/g for As(V). According to correlation coefficient $\overline{R^2}$ values, the fitness of the models for three-, four- and five-parameter models are almost similar to each other. Thus, based on equivalent adsorption capacity, the orders followed by the models in decreasing manner are shown in Table S5 of supplementary materials. Based on the equivalent adsorption capacity values, the higher fitted model order among three-, four- and five-parameter models was Toth model with a maximum adsorption capacity of 2310.96019 mg/g for As(III) and 2845.26471 mg/g for As(V).

Table 8 represents the high adsorption capacity of metal ions reported by various researchers. Qualitatively speaking, it can be found that As(III) and As(V) loadings acquired from the present study are within the ranges obtained with other metals, though differences in the type of adsorbent/biosorbent (among other experimental conditions) utilized are of a paramount significance if quantitative comparisons must be done. Activated carbon adsorption was explored in removal of arsenic and antimony from copper electrorefining solutions [80]. A huge arsenic sorption capacity (2860 mg/g) was obtained on this coal-derived commercial carbon. The transition from surface coverage to surface precipitation is not easy to evaluate from the adsorption isotherm or to model employing estimated iron arsenic solubility. The transition occurred at varying surface coverages and dissolved arsenic concentrations. The beginning of surface precipitation happens well before monolayer coverage (assuming a mononuclear complex) [81]. In trying to differentiate between adsorption and surface precipitation in the accumulation of metal ions on solid surfaces, Sposito inferred that it is not possible to distinguish between the two phenomena based only on sorption data [82]. Rather, determination of the mechanism must be obtained through close spectroscopic determination of the molecular structure of the sorbed layer.

The descriptive models from the best to worst for As(III) and As(V) were sorted according to GoFM values and shown in Table S6 and Table S7 of supplementary materials, respectively. Among 30 different isotherm models, Vieth–Sladek isotherm was observed to be appropriate to predict the equilibrium data of biosorption/bioaccumulation of As(III) on immobilized bacterial cells according to GoFM values. However, Brouers–Sotolongo was observed to be appropriate to predict the equilibrium data of biosorption/bioaccumulation of As(V) on immobilized bacterial cells according to $\overline{R^2}$, Reduced χ^2 and Root–MSE, and Fritz–Schlunder–V was the best on the basis of R, R^2 and SSE. It signifies that the biosorption of both As(III) and As(V) does not form a multilayer on acid treated tea waste; it rather follows monolayer adsorption process and mechanism of adsorption process is complex.

Studies of Influencing Co-existing Ions

The effect of concentrations of initial co-existing ions on the biosorption/bioaccumulation process of As(III) and As(V) on *C. glutamicum* MTCC 2745 immobilized on surface of SD/$MnFe_2O_4$ composite is revealed in Figs. 13a–c and 14a–c, respectively. Consequences clearly showed that the % removal of As(III) and As(V) were observed to decrease with the presence of a very low concentration of various ions, for example copper (Cu^{2+}), zinc (Zn^{2+}), bismuth (Bi^{3+}), lead (Pb^{2+}), cobalt (Co^{2+}), nickel (Ni^{2+}), chromium (Cr^{6+}) and sulfate (SO_4^{2-}). On the other hand in the presence of iron (Fe^{3+}) and cadmium (Cd^{2+}), the removal efficiencies were observed to increase. The reduction of % removal in the existence of Cu^{2+}, Zn^2, Bi^{3+}, Pb^{2+}, Co^{2+} and Ni^{2+} ions may be clarified on the basis of the ionic radii. All these ions are bigger than As(III) and As(V) and therefore in their attendance, the %

Table 8 Metal loadings on various adsorbents/biosorbents

Metal	Adsorbent/biosorbent	Adsorption capacity (mg/g)	Remarks	References
Gold	Activated carbon	1380	Cortez Gold Mines coconut shell-activated carbon	[76]
Gold	Activated carbon	3400	Harmony No. 4 Plant 1 stage of seven-stages CIP circuit	[77]
Molybdenum	Activated carbon	160	pH 2.0	[76]
Molybdenum	Activated carbon	130	Spent acid effluent	
Copper	Chitosan–Fe–S–C	413.20	Carbonaceous sulfur-containing chitosan–Fe(III)	[78]
Copper	Tailor-made composite adsorbent	200.80	Wastewater	[79]
Arsenic	Activated carbon	2860	Copper electrorefining solution	[80]
Arsenic (As(III)/As(V))	*C. glutamicum* MTCC 2745 immobilized on SD/$MnFe_2O_4$ composite	1672.322 for As(III) and 1861.715 for As(V)	Synthetic wastewater	Present study

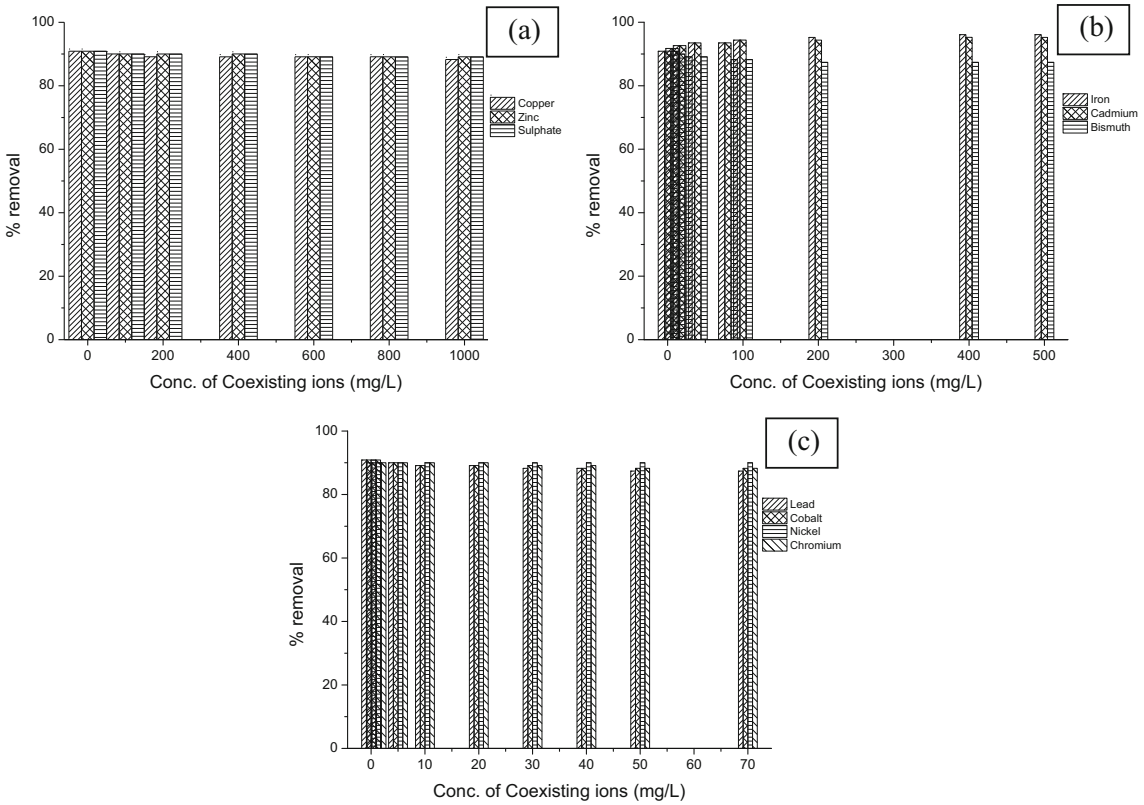

Fig. 13 Effect of co-existing ions **a** copper, zinc and sulfate; **b** iron, cadmium and bismuth and **c** lead, cobalt, nickel and chromium on the removal of As(III) (C_o: 50 mg/L; M: 1 g/L; pH: 7; t: 240 min; T: 30 °C)

removal reduced [53, 83, 84]. This might be owing to the competition of these ions with arsenic for the biosorption sites and/or owing to masking of biosorption sites by the bigger ions [85]. Conversely, the ionic radii of Cd^{2+} and Fe^{3+} are almost the same, so there was no reducing effect [85]. The % removal of As(III) and As(V) increased in presence of both Cd^{2+} and Fe^{3+} ions. Mostly, Cd^{2+} and Fe^{3+} ions could be biosorbed/bioaccumulated by immobilized bacterial cells and efficiently compensated the surface negative charge generated by specific biosorption/bioaccumulation of As(III) and As(V) and acted as a bridge between immobilized bacterial cells and As(III) and As(V) ions, which has preferred the biosorption/bioaccumulation of As(III) and As(V) anions [83, 84]. While the ionic radius of Cd^{2+} is nearly the same, so there was no reducing effect [53]. As well as this, Fe^{3+} ions being an outstanding adsorbent for arsenic, the current effect in the occurrence of Fe^{3+} may also be owing to adsorption of arsenic onto ferric hydroxides ($Fe(OH)_3$) that would form while Fe^{3+} ions are present in wastewater under oxic conditions [86]. Sulfate is divalent oxyanion and has competition with anions of both As(III) and As(V) through enhanced electrostatic interaction [87]. Sulfate is divalent oxyanion and has competition with anions of both As(III) and As(V) through enhanced electrostatic interaction [87]. Sulfate had a negligible influence on As(III) and As(V) biosorption/bioaccumulation. This is due to the fact that the sulfate binding affinity for the immobilized bacterial cells is much weaker than arsenic [48, 88, 89]. These consequences are also consistent with other study [90, 91].

Desorption Studies

In biosorption/bioaccumulation process, heavy metals are biosorbed/bioaccumulated on *C. glutamicum* MTCC 2745 immobilized on surface of SD/$MnFe_2O_4$ composite. With the time of shaking, the bacterial cells consume more arsenic and die. So, a large amount of biomass is produced and the immobilized bacterial cells lose its activity. Loss on biosorption capacity is also attained because of the blockage of pores of the biosorbents attached with biofilm due to the biosorption/bioaccumulation of metals/metalloids and growth of biomass. So, desorption of biosorbed heavy metals from the metal–loaded biosorbent or regeneration of the biosorbent is mandatory.

Desorption of biosorbed/bioaccumulated As(III) and As(V) from the arsenic-loaded immobilized bacterial cells was performed using different concentrations of NaOH solution. The results are shown in Fig. 15. It is agreed that while the concentration of NaOH was about 0.05 M, the rate of desorption of As(III) and As(V) improved with the rise in alkalinity and grasped a maximal of 81.34 and 88.727 %, respectively. Then, rate of desorption reduced with further rise

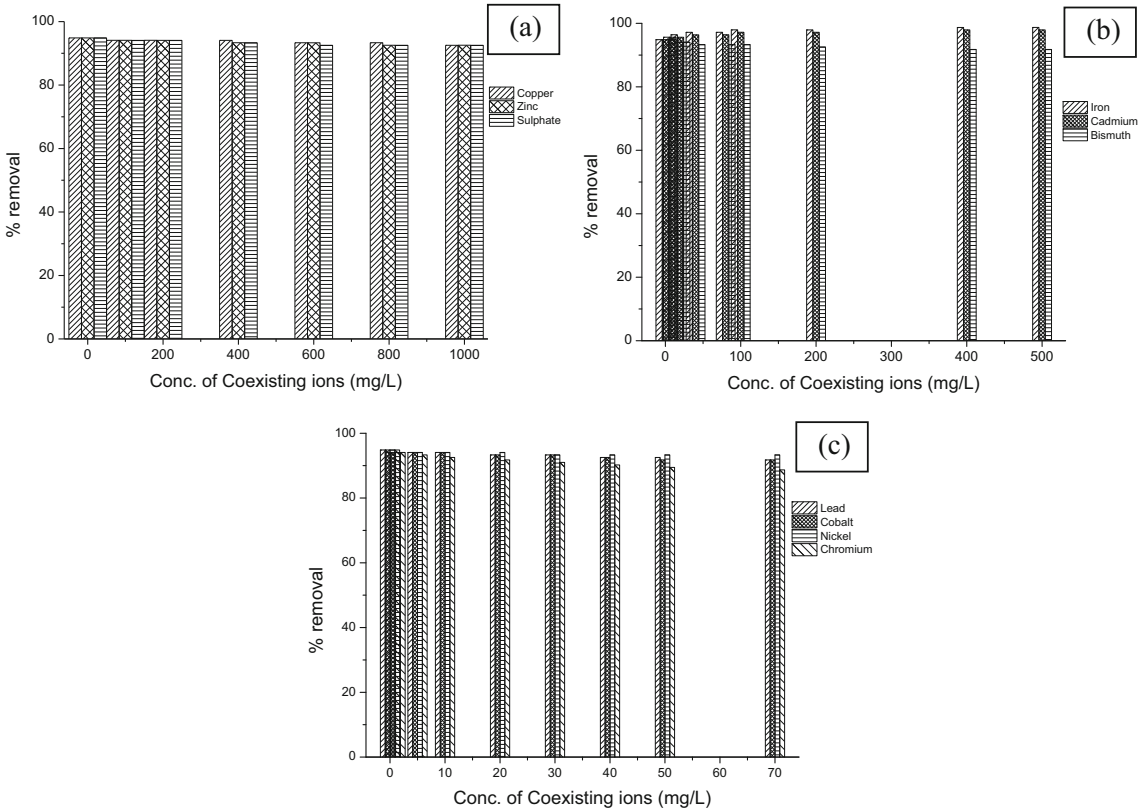

Fig. 14 Effect of co-existing ions **a** copper, zinc and sulfate; **b** iron, cadmium and bismuth and **c** lead, cobalt, nickel and chromium on the removal of As(V) (C_o: 50 mg/L; M: 1 g/L; pH: 4; t: 240 min; T: 30 °C)

in alkalinity. The lower rate of desorption exposed that the As(III) and As(V) biosorption/bioaccumulation on the surface of immobilized bacterial cells are partially reversible, because of the strong adsorptive interactions between As(III) and As(V) and the surfaces of the immobilized bacterial cells. The surface hydroxyl groups became deprotonated and negatively charged at high pH, causing an efficient desorption of negatively charged arsenic species. So, NaOH solution was utilized for desorption of the adsorbed arsenic from immobilized bacterial cells [92]. Then, the main possible desorption reaction could be summarized as:

$$MeOH_2^+ \cdots\cdots AsO_3^{3-} + OH^- \rightarrow MeOH + AsO_3^{3-} + H_2O \quad (25)$$

$$MeOH_2^+ \cdots\cdots O_3AsH_2 + OH^- \rightarrow MeOH + H_2AsO_3^{3-} + H_2O \quad (26)$$

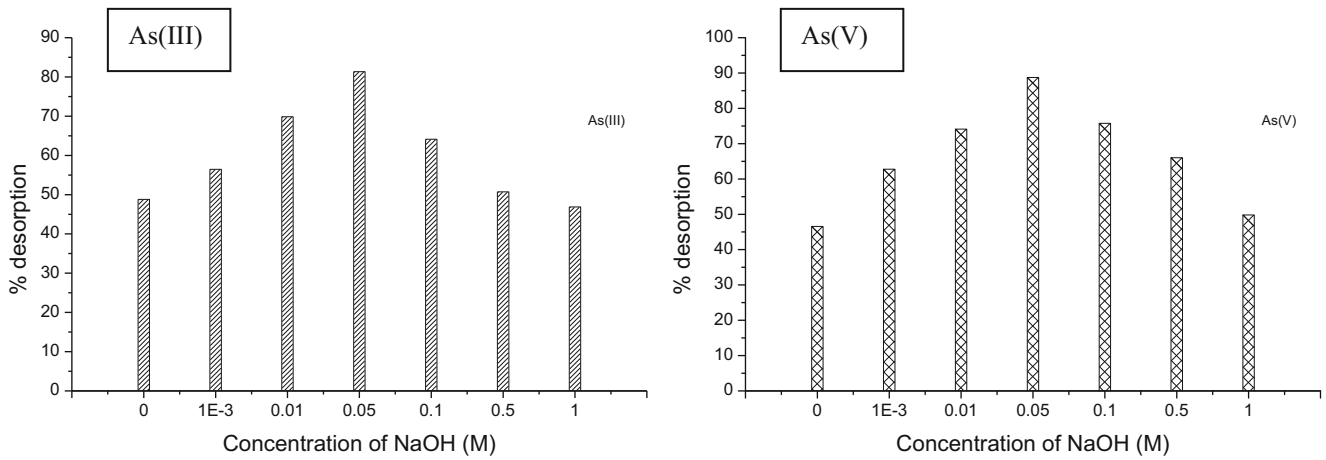

Fig. 15 Desorption of As(III) and As(V) from *C. glutamicum* MTCC 2745 immobilized on surface of SD/$MnFe_2O_4$ composite using different concentrations of NaOH solution (exhausted M: 1 g/L, t:240 min, T: 30 °C)

$$MeOH_2^+ \cdots\cdots AsO_4^{3-} + OH^- \rightarrow MeOH + AsO_4^{3-} + H_2O \quad (27)$$

$$MeOH_2^+ \cdots\cdots {}^-O_4AsH_2 + OH^- \rightarrow MeOH + H_2AsO_4^{3-} + H_2O \quad (28)$$

$$Me^+ \cdots\cdots AsO_3^{3-} + OH^- \rightarrow MeOH + AsO_3^{3-} \quad (29)$$

$$Me{-}OAsO_3H_2 + OH^- \rightarrow MeOH + H_2AsO_3^{3-} \quad (30)$$

$$Me^+ \cdots\cdots AsO_4^{3-} + OH^- \rightarrow MeOH + AsO_4^{3-} \quad (31)$$

$$Me{-}OAsO_4H_2 + OH^- \rightarrow MeOH + H_2AsO_4^{3-} \quad (32)$$

Advantage of Simultaneous Biosorption and Bioaccumulation Study

The adherence of the bacterial cells to SD/$MnFe_2O_4$ composite particles was found through SEM studies (Fig. 2e, g). The cell wall structure of the microbes had numerous sites and complexity for the uptake of metal ions. Biosorption of thorium and uranium by *R. arrhizus* not only involved physical adsorption but also the complex formations. At this point, the complex involved was the metal ion with hydroxyl group of EPS and the nitrogen of the chitin cell wall network and the hydrolysis of complex and precipitation of the hydrolysis product in the cell wall [93]. Immobilization of bacterial cells onto the surface of a non-living carrier, like SD/$MnFe_2O_4$ composite through physical adsorption, electrostatic forces or covalent bonding between the cell membrane and the carrier was a beneficial method. The photomicrographs of the bacterial cells absorbed onto the surface of SD/$MnFe_2O_4$ composite particles exposed that SD/$MnFe_2O_4$ composite particles have many crevices which perform as a den for the microbial cells. This defends the bacterial cells from direct exposure to high concentration of the poisonous metal due to which there is a rise in the metal uptake capacity of the bacterial cells [22]. Andrews and Tien recommended that the formation of microbial monolayer on the surface of a solid carrier includes a complex mechanism for the elimination of target element from the liquid medium [94]. In the presence of microbial film, the mechanism of removal of substances includes (i) the transport of substance, like metal ions from bulk liquid to the microbial monolayer surface, (ii) simultaneous mass transfer, biosorption of ions on the surface, biochemical reaction inside the microbial monolayer film and (iii) simultaneous mass transfer and biosorption inside the biosorbent [94]. Dynamic nature of the microbial film increases the complexity [11]. In SBB, the presence of solid carrier increases the liquid–solid surfaces, on which microbial cells, organic materials, enzymes and oxygen are adsorbed providing an enriched environment for microbial metabolism [11, 94]. Thus, the SBB process was found to be much more efficient than that of biosorption alone.

It is very difficult to compare directly the adsorbent capacity of studied adsorbents with other adsorbents capacity stated in the literature because of the changing operating conditions used in those studies; yet, *C. glutamicum* MTCC 2745 immobilized on SD/$MnFe_2O_4$ composite used in this research have higher adsorption capacity compare to other adsorbents. The adsorption capacity differences of As(III) and As(V) ions uptake are attributed to the properties of each adsorbent for instance adsorbent structure, functional groups and surface area [95].

Table 9.

Conclusions

- In this study, *C. glutamicum* MTCC 2745 immobilized on surface of SD/$MnFe_2O_4$ composite excellently was employed to remove As(III) and As(V) from synthetically prepared wastewater and showed high elimination efficiency.
- FT-IR analysis recommended that Fe–O, Mn–O, Me–OH bond (Me stands for $MnFe_2O_4$ and surface of bacteria) of *C. glutamicum* MTCC 2745 immobilized on surface of

Table 9 Maximum adsorption capacities (q_m, mg/g) of As(III) and As(V) of immobilized bacterial cells compared with other adsorbents (in mg per g of solid material)

Adsorbent	pH	As(III)	pH	As(V)	References
C. rhizoma	–	–	8.0	22.04	[91]
W. frutescens	–	–	8.0	16.88	[91]
Inonotus hispidus biomass	6.0	51.9	2.0	59.6	[96]
Zr(IV)–loaded orange waste	9.0	130.0	–	–	[97]
Lassonia nigrescens	–	–	2.5	45.2	[98]
Zirconium–loaded adsorbent	–	–	2.0	149.8	[99]
Fe(III)–loaded cellulose	9.0	18.0	4.5	137.1	[100]
Chitosan	–	–	4.0	58	[101]
Iron(III)–loaded LDA	9.0	62.9	3.5	55.7	[102]
C. glutamicum MTCC 2745 immobilized on SD/$MnFe_2O_4$ composite	7.0	1672.322	7.0	1861.715	This study

$SD/MnFe_2O_4$ composite were credited to the good biosorption/bioaccumulation.

- The optimum pH for As(III) and As(V) biosorption/bioaccumulation process with *C. glutamicum* MTCC 2745 immobilized on surface of $SD/MnFe_2O_4$ composite is 7.
- The biosorption/bioaccumulation mechanism of As(III) and As(V) on the *C. glutamicum* MTCC 2745 immobilized on surface of $SD/MnFe_2O_4$ composite was complex. Electrostatic interaction happened in biosorption/bioaccumulation of As(III) and As(V) and the hydroxyl groups bonded to $MnFe_2O_4$ and surface of bacteria played a significant role in the biosorption/bioaccumulation of As(III) and As(V) via electrostatic interaction or ligand exchange.
- The optimum biosorbent dose and contact time for biosorption/bioaccumulation of As(III) and As(V) are 1 g/L and 240 min, respectively.
- The rate of biosorption/bioaccumulation of both As(III) and As(V) by *C. glutamicum* MTCC 2745 immobilized on surface of $SD/MnFe_2O_4$ composite has reduced with rising concentration.
- Cd^{2+} and Fe^{3+} ions present in copper smelting wastewater exhibited positive influence on biosorption of As(III) and As(V) by that biosorbent attached with biofilm while other ions such as Cu^{2+}, Zn^2, Bi^{3+}, Pb^{2+}, Co^{2+}, Ni^{2+} and Cr^{6+}, and $SO_4{}^{2-}$ had negative influence on scavenging of As(III) and As(V) by that biosorbent attached with biofilm.
- Biosorbed/Bioaccumulated As(III) and As(V) Could Be Efficiently Desorbed by 0.05 M NaOH Solution.
- By applying 30 different isotherm models and using method of the non-linear regression for curve fitting analysis (maximizing the correlation coefficient (R, R^2, $\overline{R^2}$) and minimizing the error values (SSE, Reduced χ^2 and Root–MSE)) to evaluate optimum parameter sets, the Vieth–Sladek isotherm was the best fit isotherm for As(III) while the Brouers–Sotolongo isotherm (according to $\overline{R^2}$, Reduced χ^2 and Root–MSE) as well as Fritz–Schlunder–V (according to R, R^2 and SSE) were observed suitable to forecast the equilibrium data of biosorption/bioaccumulation of As(V) onto *C. glutamicum* MTCC 2745 immobilized on surface of $SD/MnFe_2O_4$ composite. It specifies that the biosorption/bioaccumulation of both As(III) and As(V) does not form a multilayer on *C. glutamicum* MTCC 2745 immobilized on surface of $SD/MnFe_2O_4$ composite; it rather follows monolayer biosorption/bioaccumulation process and mechanism of biosorption/bioaccumulation process is complex.
- On the basis of $\overline{R^2}$ values, the highest fitted model order among one and two-parameter models is Langmuir model with a maximum adsorption capacity of 1672.3221 mg/g for As(III) and 1861.7145 mg/g for As(V).
- Based on the equivalent adsorption capacity values, the higher fitted model order among three-, four- and five-parameter models is Toth model with a maximum adsorption capacity of 2310.96 mg/g for As(III) and 2845.265 mg/g for As(V).
- From Dubinin–Radushkevich model, it was determined that the adsorption of As(III) and As(V) by *C. glutamicum* MTCC 2745 immobilized on surface of $SD/MnFe_2O_4$ composite may be an ion exchange and spontaneous process.
- *C. glutamicum* MTCC 2745 immobilized on surface of $SD/MnFe_2O_4$ composite, hybrid biosorbent has a potential application for elimination of arsenic in water treatment.

A_E the energy of adsorption (KJ/mol), A_{FS} Fritz–Schlunder–IV isotherm constant ((mg/g)(L/mg)$^{\alpha FS}$), a_{FS} Fritz–Schlunder–IV model exponent, a_K Khan isotherm exponent, A_{KC} Koble–Corrigan parameters ((mg/g)(L/mg)^{nKC}), b_B Baudu isotherm constant (L/mg), B_{FS} Fritz–Schlunder–IV isotherm constant ((L/mg)$^{\beta FS}$), b_{FS} Fritz–Schlunder–IV model exponent, b_J Jossens model exponent, b_K Khan isotherm constant (L/mg), B_{KC} Koble–Corrigan parameters ((L/g)^{nKC}), b_{TE} Temkin isotherm constant corresponding to heat of adsorption (J/mol), C_0 initial concentration of arsenic in the solution (mg/L), C_e equilibrium concentration of arsenic in the solution (mg/L), E mean free energy (KJ/mol), K_1 Fritz–Schlunder–V equilibrium constant ((L/mg)$^{\alpha FS}$), K_2 Fritz–Schlunder–V equilibrium constant ((L/mg)$^{\beta FS}$), K_{BS} Brouers–Sotolongo isotherm constant ((mg/g)(L/mg)$^{1/\alpha}$), K_F Freundlich isotherm constant ((mg/g)(L/mg)$^{1/nF}$), K_{DR} Dubinin–Radushkevich isotherm constant or activity coefficient linked to mean adsorption energy (mol^2/KJ^2), K_{FS} Fritz–Schlunder–III isotherm constant ((L/mg)$^n{}_{FS}$), K_H Hill isotherm constant (L/g), K_{HE} adsorption equilibrium constant known as Henry constant (L/g), K_{HK} Holl–Krich isotherm constant ((L/mg)^{nHK}), K_L Langmuir isotherm constant signifying the affinity between the adsorbent and the adsorbate molecules relating the energy of adsorption (L/mg), K_{LJF} Langmuir–Freundlich–Jovanovic isotherm constant (L/mg), K_J Jossens isotherm constant ((mg/g)(L/mg)), K_{JF} Jovanovic–Freundlich isotherm constant depends only on the temperature (L/mg), K_{JV} Jovanovic isotherm constant linked to the free energy of adsorption (L/g), K_L Langmuir isotherm constant (L/mg), K_{LF} Langmuir–Freundlich isotherm constant (L/mg), K_{LJ} Langmuir–Jovanovic isotherm constant (L/mg), K_m Activated sludge model constant (L/g), K_{MJ} Marczewski–Jaroniec isotherm constant (L/mg), K_{RP} Redlich–Peterson isotherm constant (L/g), K_{RPI} Radke–Prausnitz I isotherm constant (L/mg), K_{RPII} Radke–Prausnitz II isotherm constant (L/mg), K_{RPIII} Radke–Prausnitz III isotherm constant (L/mg), K_S Sips isotherm constant related to affinity constant (mg/L$^{)-1/m}{}_S$, K_T Toth isotherm constant linked to affinity constant (L/mg), K_{TE} Temkin isotherm constant corresponding to the maximum binding energy (L/mg), K_U Unilan isotherm constant ((L/

mg)^{bHK}), K_{VS} Vieth–Sladek isotherm constant (L/mg), J Jossens isotherm constant ((L/mg)^{bJ}), M mass of the adsorbent (dry) used (g), m_{LF} Langmuir–Freundlich model exponent or heterogeneity factor, m_{MJ} Marczewski–Jaroniec model exponent, m_{RPI} Radke–Prausnitz I model exponent, m_{RPII} Radke–Prausnitz II model exponent, m_{RPIII} Radke–Prausnitz III model exponent, m_s Sips model exponent, n the number of observations in the experimental study, n_F Freundlich model exponent, n_{FS} Fritz–Schlunder–III model exponent, n_H Hill cooperativity coefficient, n_{HK} Holl–Krich model exponent, n_{JF} Jovanovic–Freundlich model exponent, n_{LJ} Langmuir–Jovanovic model exponent, n_{LJF} Langmuir–Freundlich–Jovanovic model exponent, n_{KC} Koble–Corrigan parameters, N_m Activated sludge model exponential constant, n_{MJ} Marczewski–Jaroniec model exponent, n_T Toth isotherm exponent, a measure of surface heterogeneity, p the number of parameters to be determined, q_e adsorption capacity or amount of arsenic adsorbed onto the surface of adsorbent at equilibrium (mg/g), $q_{e,exp}$ the equilibrium adsorption capacity observed from the batch experiment (mg/g), $q_{e,model}$ the prediction from the isotherm model corresponding to C_e (mg/g), q_{mB} maximum monolayer adsorption capacity predicted by Baudu isotherm (mg/g), q_{mBS} maximum monolayer adsorption capacity forecasted by Brouers–Sotolongo isotherm (mg/g), q_{mDR} maximum monolayer adsorption capacity predicted by Dubinin–Radushkevich isotherm (mg/g), q_{mFS} maximum monolayer adsorption capacity forecasted by Fritz–Schlunder–III isotherm (mg/g), q_{mFS5} maximum monolayer adsorption capacity given by Fritz–Schlunder–V isotherm (mg/g), q_{mH} maximum monolayer adsorption capacity predicted by Hill isotherm (mg/g), q_{mHK} maximum monolayer adsorption capacity predicted by Holl–Krich isotherm (mg/g), q_{mJF} maximum monolayer adsorption capacity predicted by Jovanovic–Freundlich isotherm (mg/g), q_{mJV} maximum monolayer adsorption capacity predicted by Jovanovic isotherm (mg/g), q_{mK} maximum monolayer adsorption capacity forecasted by Khan isotherm (mg/g), q_{mL} maximum monolayer adsorption capacity predicted by Langmuir isotherm (mg/g), q_{mLF} maximum monolayer adsorption capacity predicted by Langmuir–Freundlich isotherm (mg/g), q_{mLFJ} maximum monolayer adsorption capacity predicted by Langmuir–Freundlich–Jovanovic isotherm (mg/g), q_{mLJ} maximum monolayer adsorption capacity predicted by Langmuir–Jovanovic isotherm (mg/g), q_{mMJ} maximum monolayer adsorption capacity forecasted by Marczewski–Jaroniec isotherm (mg/g), q_{mL} maximum monolayer adsorption capacity predicted by Langmuir isotherm (mg/g), q_{mRPI} maximum monolayer adsorption capacity forecasted by Radke–Prausnitz I isotherms (mg/g), q_{mRPII} maximum monolayer adsorption capacity forecasted by Radke–Prausnitz II isotherms (mg/g), q_{mRPIII} maximum monolayer adsorption capacity forecasted by Radke–Prausnitz III isotherms (mg/g), q_{mS} maximum monolayer adsorption capacity predicted by Sips isotherm (mg/g), q_{mT} maximum monolayer adsorption capacity forecasted by Toth isotherm (mg/g), q_{mU} maximum monolayer adsorption capacity forecasted by Unilan isotherm (mg/g), q_{mVS} maximum monolayer adsorption capacity predicted by Vieth–Sladek isotherm (mg/g), R universal gas constant (8.314 J/mol K), R_d distribution coefficient, R_e removal efficiency, R_L separation factor or adsorption intensity, s Unilan model exponent dependent on temperature describing the heterogeneity of the system, T absolute temperature (K), V working volume of the solution (L), x Baudu model exponent, y Baudu model exponent, α Brouers–Sotolongo model exponent, α_{FS} Fritz–Schlunder–V model exponent, α_{RP} Redlich–Peterson isotherm constant (L/mg)$^{\beta RP}$, β_{FS}, Fritz–Schlunder–V model exponent, β_{RP}, Redlich–Peterson model exponent, β_{VS} Vieth–Sladek equilibrium constant, ε Polanyi potential (mol^2/KJ^2)

Acknowledgments The authors would like to thank the Indian Institute of Technology, Roorkee for providing necessary facilities and to Ministry of Human Resource Development, Government of India for financial support. The thoughtful comments by Dr. Meng Nan Chong, the Editor and two anonymous reviewers are highly appreciated.

References

1. Smedley PL, Kinniburgh DG (2002) A review of the source, behaviour and distribution of arsenic in natural waters. Appl Geochem 17(5):517–568. doi:10.1016/S0883-2927(02)00018-5
2. Mohan D, Pittman CU (2007) Arsenic removal from water/wastewater using adsorbents—a critical review. J Hazard Mater 142(1):1–53. doi:10.1016/j.jhazmat.2007.01.006
3. Mondal P, Majumder CB, Mohanty B (2006) Laboratory based approaches for arsenic remediation from contaminated water: recent developments. J Hazard Mater 137(1):464–479. doi:10.1016/j.jhazmat.2006.02.023
4. Basha CA, Bhadrinarayana NS, Anantharaman N, Begum KM (2008) Heavy metal removal from copper smelting effluent using electrochemical cylindrical flow reactor. J Hazard Mater 152(1):71–78. doi:10.1016/j.jhazmat.2007.06.069
5. Basha CA, Selvi SJ, Ramasamy E, Chellammal S (2008) Removal of arsenic and sulphate from the copper smelting industrial effluent. Chem Eng J 141(1):89–98. doi:10.1016/j.cej.2007.10.027
6. WHO (1993) Guidelines for drinking water quality. World Health Organization, Geneva, p 41
7. European commission Directive (1998) 98/83/EC, related with drinking water quality intended for human consumption. Brussels.
8. Nishimura T, Robins RG (1998) A re-evaluation of the solubility and stability regions of calcium arsenites and calcium arsenates in aqueous solution at 25 °C. Miner Process Extr Metall Rev 18(3–4):283–308. doi:10.1080/08827509808914159
9. Luo T, Cui J, Hu S, Huang Y, Jing C (2010) Arsenic removal and recovery from copper smelting wastewater using TiO_2. Environ Sci Technol 44(23):9094–9098. doi:10.1021/es1024355
10. Owlad M, Aroua MK, Daud WA, Baroutian S (2009) Removal of hexavalent chromium-contaminated water and wastewater: a review. Water Air Soil Pollut 200(1–4):59–77. doi:10.1007/s11270-008-9893-7
11. Jain S, Vyas RK, Pandit P, Dalai AK (2014) Adsorption of antiviral drug, acyclovir from aqueous solution on powdered activated charcoal: kinetics, equilibrium, and thermodynamic studies. Desalin Water Treat 52(25–27):4953–4968. doi:10.1080/19443994.2013.810324

12. Roshan Dash R, Balomajumder C, Kumar A (2009) Removal of metal cyanides from aqueous solutions by suspended and immobilized cells of *Rhizopus oryzae* (MTCC 2541). Eng Life Sci J 9(1):53–59. doi:10.1002/elsc.200700024
13. Velásquez L, Dussan J (2009) Biosorption and bioaccumulation of heavy metals on dead and living biomass of *Bacillus sphaericus*. J Hazard Mater 167(1):713–716. doi:10.1016/j.jhazmat.2009.01.044
14. Giri AK, Patel RK, Mahapatra SS (2011) Artificial neural network (ANN) approach for modelling of arsenic (III) biosorption from aqueous solution by living cells of *Bacillus cereus* biomass. Chem Eng J 178:15–25. doi:10.1016/j.cej.2011.09.111
15. Giri AK, Patel RK, Mahapatra SS, Mishra PC (2013) Biosorption of arsenic (III) from aqueous solution by living cells of *Bacillus cereus*. Environ Sci Pollut Res 20(3):1281–1291. doi:10.1007/s11356-012-1249-6
16. Sarı A, Uluozlü ÖD, Tüzen M (2011) Equilibrium, thermodynamic and kinetic investigations on biosorption of arsenic from aqueous solution by algae (*Maugeotia genuflexa*) biomass. Chem Eng J 167(1):155–161. doi:10.1016/j.cej.2010.12.014
17. Prasad KS, Srivastava P, Subramanian V, Paul J (2011) Biosorption of As (III) ion on *Rhodococcus* sp. WB-12: biomass characterization and kinetic studies. Sep Sci Technol 46(16): 2517–2525. doi:10.1016/j.cej.2010.12.014
18. Prasad KS, Ramanathan AL, Paul J, Subramanian V, Prasad R (2013) Biosorption of arsenite (As^{+3}) and arsenate (As^{+5}) from aqueous solution by *Arthrobacter* sp. biomass. Environ Technol 34(19):2701–2708. doi:10.1080/09593330.2013.786137
19. Gadd GM (1992) Molecular biology and biotechnology of microbial interactions with organic and inorganic heavy metal compounds. In: Herber RA, Sharp RJ (eds) Molecular biology and biotechnology of extremophiles. Blackie and Sons, Glasgow, pp 225–257
20. Mondal P, Majumder CB, Mohanty B (2008) Treatment of arsenic contaminated water in a batch reactor by using *Ralstonia eutropha* MTCC 2487 and granular activated carbon. J Hazard Mater 153(1):588–599. doi:10.1016/j.jhazmat.2007.09.028
21. Quintelas C, Fernandes B, Castro J, Figueiredo H, Tavares T (2008) Biosorption of Cr (VI) by three different bacterial species supported on granular activated carbon—a comparative study. J Hazard Mater 153(1):799–809. doi:10.1016/j.jhazmat.2007.09.027
22. Mishra V, Balomajumder C, Agarwal VK (2013) Design and optimization of simultaneous biosorption and bioaccumulation (SBB) system: a potential method for removal of Zn (II) ion from liquid phase. Desalin Water Treat 51(16–18):3179–3188. doi:10.1080/19443994.2012.749027
23. Kim HC, Lee CG, Park JA, Kim SB (2010) Arsenic removal from water using iron-impregnated granular activated carbon in the presence of bacteria. J Environ Sci Heal A 45(2):177–182. doi:10.1080/10934520903429832
24. Mateos LM, Ordóñez E, Letek M, Gil JA (2006) "Corynebacterium glutamicum" as a model bacterium for the bioremediation of arsenic. Int Microbiol 9(3):207–216
25. Kotrba P, Dolečková L, de Lorenzo V, Ruml T (1999) Enhanced bioaccumulation of heavy metal ions by bacterial cells due to surface display of short metal binding peptides. Appl Environ Microbiol 65(3):1092–1098
26. Valls M, Atrian S, de Lorenzo V, Fernández LA (2000) Engineering a mouse metallothionein on the cell surface of *Ralstonia eutropha* CH34 for immobilization of heavy metals in soil. Nat Biotechnol 18(6):661–665. doi:10.1038/76516
27. Sidiras D, Batzias F, Schroeder E, Ranjan R, Tsapatsis M (2011) Dye adsorption on autohydrolyzed pine sawdust in batch and fixed-bed systems. Chem Eng J 171(3):883–896. doi:10.1016/j.cej.2011.04.029
28. Goldberg S, Johnston CT (2001) Mechanisms of arsenic adsorption on amorphous oxides evaluated using macroscopic measurements, vibrational spectroscopy, and surface complexation modeling. J Colloid Interface Sci 234(1):204–216. doi:10.1006/jcis.2000.7295
29. Parsons JG, Lopez ML, Peralta-Videa JR, Gardea-Torresdey JL (2009) Determination of arsenic (III) and arsenic (V) binding to microwave assisted hydrothermal synthetically prepared Fe_3O_4, Mn_3O_4, and $MnFe_2O_4$ nanoadsorbents. Microchem J 91(1):100–106. doi:10.1016/j.microc.2008.08.012
30. Ncibi MC (2008) Applicability of some statistical tools to predict optimum adsorption isotherm after linear and non-linear regression analysis. J Hazard Mater 153(1):207–212. doi:10.1016/j.jhazmat.2007.08.038
31. Hadi M, McKay G, Samarghandi MR, Maleki A, Solaimany Aminabad M (2012) Prediction of optimum adsorption isotherm: comparison of chi-square and Log-likelihood statistics. Desalin Water Treat 49(1–3):81–94. doi:10.1080/19443994.2012.708202
32. Edgar TF, Himmelblau DM (1989) Optimization of chemical processes. McGraw–Hill, New York
33. Hanna OT, Sandall OC (1995) Computational methods in chemical engineering. Prentice–Hall International, New Jersey
34. Allievi MC, Mariano PA (2011) Metal biosorption by surface-layer proteins from *Bacillus* species. J Microbiol Biotechnol 21(2):147–153. doi:10.4014/jmb.1009.09046
35. Singha B, Das SK (2011) Biosorption of Cr (VI) ions from aqueous solutions: kinetics, equilibrium, thermodynamics and desorption studies. Colloids Surf B 84(1):221–232. doi:10.1016/j.colsurfb.2011.01.004
36. Seki H, Suzuki A, Maruyama H (2005) Biosorption of chromium (VI) and arsenic (V) onto methylated yeast biomass. J Colloid Interface Sci 281(2):261–166. doi:10.1016/j.jcis.2004.08.167
37. Kumari P, Sharma P, Srivastava S, Srivastava MM (2006) Biosorption studies on shelled *Moringa oleifera* Lamarck seed powder: removal and recovery of arsenic from aqueous system. Int J Miner Process 78(3):131–139. doi:10.1016/j.minpro.2005.10.001
38. François F, Lombard C, Guigner JM, Soreau P, Brian-Jaisson F, Martino G, Vandervennet M, Garcia D, Molinier AL, Pignol D, Peduzzi J (2012) Isolation and characterization of environmental bacteria capable of extracellular biosorption of mercury. Appl Environ Microbiol 78(4):1097–1106. doi:10.1128/AEM.06522-11
39. Baciocchi R, Chiavola A, Gavasci R (2005) Ion exchange equilibria of arsenic in the presence of high sulphate and nitrate concentrations. Water Sci Technol Water Supply 5(5):67–74
40. Merroun ML, Raff J, Rossberg A, Hennig C, Reich T, Selenska-Pobell S (2005) Complexation of uranium by cells and S-layer sheets of *Bacillus sphaericus* JG-A12. Appl Environ Microbiol 71(9):5532–5543. doi:10.1128/AEM.71.9.5532-5543.2005
41. Pokhrel D, Viraraghavan T (2008) Arsenic removal from an aqueous solution by modified A. Niger biomass: batch kinetic and isotherm studies. J Hazard Mater 150(3):818–825. doi:10.1016/j.jhazmat.2007.05.041
42. McCafferty E (2010) Relationship between the isoelectric point (pH pzc) and the potential of zero charge (E pzc) for passive metals. Electrochim Acta 55(5):1630–1637. doi:10.1016/j.electacta.2009.10.040
43. Ren Y, Li N, Feng J, Luan T, Wen Q, Li Z, Zhang M (2012) Adsorption of Pb (II) and Cu (II) from aqueous solution on magnetic porous ferrospinel $MnFe_2O_4$. J Colloid Interface Sci 367(1): 415–421. doi:10.1016/j.jcis.2011.10.022
44. Kohler T, Armbruster T, Libowitzky E (1997) Hydrogen bonding and Jahn–Teller distortion in groutite, α-MnOOH, and manganite, γ-MnOOH, and their relations to the manganese dioxides

ramsdellite and pyrolusite. J Solid State Chem 133(2):486–500. doi:10.1006/jssc.1997.7516
45. Parida KM, Mallick S, Mohapatra BK, Misra VN (2004) Studies on manganese-nodule leached residues: 1. Physicochemical characterization and its adsorption behavior toward Ni^{2+} in aqueous system. J Colloid Interface Sci 277(1):48–54. doi:10.1016/j.jcis.2004.04.057
46. Li Z, Deng S, Yu G, Huang J, Lim VC (2010) As (V) and As (III) removal from water by a Ce–Ti oxide adsorbent: behavior and mechanism. Chem Eng J 161(1):106–113. doi:10.1016/j.cej.2010.04.039
47. Mondal P, Balomajumder C, Mohanty B (2007) A laboratory study for the treatment of arsenic, iron, and manganese bearing ground water using Fe^{3+} impregnated activated carbon: effects of shaking time, pH and temperature. J Hazard Mater 144(1):420–426. doi:10.1016/j.jhazmat.2006.10.078
48. Zhang G, Liu H, Liu R, Qu J (2009) Adsorption behavior and mechanism of arsenate at Fe–Mn binary oxide/water interface. J Hazard Mater 168(2):820–825. doi:10.1016/j.jhazmat.2009.02.137
49. Aryal M, Ziagova M, Liakopoulou-Kyriakides M (2010) Study on arsenic biosorption using Fe (III)-treated biomass of *Staphylococcus xylosus*. Chem Eng J 162(1):178–185. doi:10.1016/j.cej.2010.05.026
50. Agarwal B, Balomajumder C, Thakur PK (2013) Simultaneous co-adsorptive removal of phenol and cyanide from binary solution using granular activated carbon. Chem Eng J 228:655–664. doi:10.1016/j.cej.2013.05.030
51. Raje N, Swain K (2002) Purification of arsenic contaminated ground water using hydrated manganese dioxide. J Radioanal Nucl Chem 253(1):77–80. doi:10.1023/A:1015812517214
52. Srivastava VC, Swamy MM, Mall ID, Prasad B, Mishra IM (2006) Adsorptive removal of phenol by bagasse fly ash and activated carbon: equilibrium, kinetics and thermodynamics. Colloid Surface A 272(1):89–104. doi:10.1016/j.colsurfa.2005.07.016
53. Baig JA, Kazi TG, Shah AQ, Kandhro GA, Afridi HI, Khan S, Kolachi NF (2010) Biosorption studies on powder of stem of *Acacia nilotica*: removal of arsenic from surface water. J Hazard Mater 178(1):941–948. doi:10.1016/j.jhazmat.2010.02.028
54. Ranjan D, Talat M, Hasan SH (2009) Biosorption of arsenic from aqueous solution using agricultural residue 'rice polish'. J Hazard Mater 166(2):1050–1059. doi:10.1016/j.jhazmat.2008.12.013
55. Bissen M, Frimmel FH (2003) Arsenic—a review. Part I: occurrence, toxicity, speciation, mobility. Acta Hydrochim Hydrobiol 31(1):9–18. doi:10.1002/aheh.200390025
56. Sengupta P, Balomajumder C (2014) Potential of corn husk leaves for the co-removal of phenol and cyanide from waste water using simultaneous adsorption and biodegradation. IJRET 3:700–707
57. Comte S, Guibaud G, Baudu M (2008) Biosorption properties of extracellular polymeric substances (EPS) towards Cd, Cu and Pb for different pH values. J Hazard Mater 151(1):185–193. doi:10.1016/j.jhazmat.2007.05.070
58. Boddu VM, Abburi K, Talbott JL, Smith ED, Haasch R (2008) Removal of arsenic (III) and arsenic (V) from aqueous medium using chitosan-coated biosorbent. Water Res 42(3):633–642. doi:10.1016/j.watres.2007.08.014
59. Karthikeyan S, Balasubramanian R, Iyer CS (2007) Evaluation of the marine algae *Ulva fasciata* and *Sargassum* sp. for the biosorption of Cu (II) from aqueous solutions. Bioresour Technol 98(2):452–455. doi:10.1016/j.biortech.2006.01.010
60. Mishra V, Balomajumder C, Agarwal VK (2012) Kinetics, mechanistic and thermodynamics of Zn (II) ion sorption: a modeling approach. Clean–Soil, Air, Water 00:1–10. doi:10.1002/clen.201100093
61. Mishra V, Balomajumder C, Agarwal VK (2010) Zn (II) ion biosorption onto surface of eucalyptus leaf biomass: isotherm, kinetic, and mechanistic modeling. Clean–Soil, Air, Water 38(11):1062–1073. doi:10.1002/clen.201000030
62. Nouri L, Ghodbane I, Hamdaoui O, Chiha M (2007) Batch sorption dynamics and equilibrium for the removal of cadmium ions from aqueous phase using wheat bran. J Hazard Mater 149(1):115–125. doi:10.1016/j.jhazmat.2007.03.055
63. Sag Y, Kutsal T (1995) Biosorption of heavy metals by *Zoogloea ramigera*: use of adsorption isotherms and a comparison of biosorption characteristics. Chem Eng J 60(1):181–188. doi:10.1016/0923-0467(95)03014-X
64. Green-Ruiz C, Rodriguez-Tirado V, Gomez-Gil B (2008) Cadmium and zinc removal from aqueous solutions by *Bacillus jeotgali*: pH, salinity and temperature effects. Bioresour Technol 99(9):3864–3870. doi:10.1016/j.biortech.2007.06.047
65. Kacar Y, Arpa Ç, Tan S, Denizli A, Genç Ö, Arıca MY (2002) Biosorption of Hg (II) and Cd (II) from aqueous solutions: comparison of biosorptive capacity of alginate and immobilized live and heat inactivated *Phanerochaete chrysosporium*. Process Biochem 37(6):601–610. doi:10.1016/S0032-9592(01)00248-5
66. Özdemir S, Kilinc E, Poli A, Nicolaus B, Güven K (2009) Biosorption of Cd, Cu, Ni, Mn and Zn from aqueous solutions by thermophilic bacteria, *Geobacillus toebii* sub. sp. *decanicus* and *Geobacillus thermoleovorans* sub. sp. *stromboliensis*: Equilibrium, kinetic and thermodynamic studies. Chem Eng J 152(1):195–206. doi:10.1016/j.cej.2009.04.041
67. Meena AK, Mishra GK, Rai PK, Rajagopal C, Nagar PN (2005) Removal of heavy metal ions from aqueous solutions using carbon aerogel as an adsorbent. J Hazard Mater 122(1):161–170. doi:10.1016/j.jhazmat.2005.03.024
68. Romero-Gonzalez J, Peralta-Videa JR, Rodrıguez E, Ramirez SL, Gardea-Torresdey JL (2005) Determination of thermodynamic parameters of Cr (VI) adsorption from aqueous solution onto *Agave lechuguilla* biomass. J Chem Thermodyn 37(4):343–737. doi:10.1016/j.jct.2004.09.013
69. Yadav KP, Tyagi BS, Pandey KK, Singh VN (1987) Fly-ash for the treatment of Cd-rich effluent. Environ Technol Lett 8:225–234
70. Roy P, Mondal NK, Das K (2014) Modeling of the adsorptive removal of arsenic: a statistical approach. J Environ Chem Eng 2(1):585–597. doi:10.1016/j.jece.2013.10.014
71. Naiya TK, Bhattacharya AK, Das SK (2009) Adsorption of Cd (II) and Pb (II) from aqueous solutions on activated alumina. J Colloid Interface Sci 333(1):14–26. doi:10.1016/j.jcis.2009.01.003
72. Vieth WR, Sladek KJ (1965) A model for diffusion in a glassy polymer. J Colloid Sci 20(9):1014–1033. doi:10.1016/0095-8522(65)90071-1
73. Dąbrowski A, Podkościelny P, Hubicki Z, Barczak M (2005) Adsorption of phenolic compounds by activated carbon—a critical review. Chemosphere 58(8):1049–1070. doi:10.1016/j.chemosphere.2004.09.067
74. Radovic LR, Moreno-Castilla C, Rivera-Utrilla J (2001) Chemistry and physics of carbon. In: Radovic LR (ed) Chemistry and physics of carbon, vol 27. Marcel Dekker, New York, pp 1–66
75. Warrens MJ (2008) On similarity coefficients for 2×2 tables and correction for chance. Psychometrika 73(3):487–502. doi:10.1007/s11336-008-9059-y
76. Gupta CK, Mukherjee TK (1990) Hydrometallurgy in extraction processes, II. CRC Press, Boca Raton, p 114
77. Marsden J, House I (1992) The chemistry of gold extraction. Ellis Horwood, Chichester, p 508
78. Wen Y, Ma J, Chen J, Shen C, Li H, Liu W (2015) Carbonaceous sulfur-containing chitosan–Fe (III): a novel adsorbent for efficient removal of copper (II) from water. Chem Eng J 259:372–380. doi:10.1016/j.cej.2014.08.011

79. Awual MR, Hasan MM (2015) Colorimetric detection and removal of copper (II) ions from wastewater samples using tailor-made composite adsorbent. Sensors Actuators B 206:692–700. doi:10.1016/j.snb.2014.09.086
80. Navarro P, Alguacil FJ (2002) Adsorption of antimony and arsenic from a copper electrorefining solution onto activated carbon. Hydrometallurgy 66(1):101–105. doi:10.1016/S0304-386X(02)00108-1
81. Li L, Stanforth R (2000) Distinguishing adsorption and surface precipitation of phosphate on goethite (α-FeOOH). J Colloid Interface Sci 230(1):12–21. doi:10.1006/jcis.2000.7072
82. Sposito G (1986) Distinguishing adsorption from surface precipitation. In: Davis JA, Hayes KF (eds) Geochemical processes at mineral surfaces, vol 323, ACS symposium series., pp 217–228
83. Dambies L, Guibal E, Roze A (2000) Arsenic (V) sorption on molybdate-impregnated chitosan beads. Colloids Surf A 170(1):19–31. doi:10.1016/S0927-7757(00)00484-2
84. Pandey PK, Choubey S, Verma Y, Pandey M, Chandrashekhar K (2009) Biosorptive removal of arsenic from drinking water. Bioresour Technol 100:634–637. doi:10.1016/j.biortech.2008.07.063
85. Maliyekkal SM, Philip L, Pradeep T (2009) As (III) removal from drinking water using manganese oxide-coated-alumina: performance evaluation and mechanistic details of surface binding. Chem Eng J 153(1):101–107. doi:10.1016/j.cej.2009.06.026
86. Kundu S, Gupta AK (2006) Adsorptive removal of As (III) from aqueous solution using iron oxide coated cement (IOCC): evaluation of kinetic, equilibrium and thermodynamic models. Sep Purif Technol 51(2):165–172. doi:10.1016/j.seppur.2006.01.007
87. Awual MR, Jyo A, Ihara T, Seko N, Tamada M, Lim KT (2011) Enhanced trace phosphate removal from water by zirconium (IV) loaded fibrous adsorbent. Water Res 45(15):4592–4600. doi:10.1016/j.watres.2011.06.009
88. Zhang G, Qu J, Liu H, Liu R, Wu R (2007) Preparation and evaluation of a novel Fe–Mn binary oxide adsorbent for effective arsenite removal. Water Res 41(9):1921–1928. doi:10.1016/j.watres.2007.02.009
89. Yu X, Tong S, Ge M, Zuo J, Cao C, Song W (2013) One-step synthesis of magnetic composites of cellulose@ iron oxide nanoparticles for arsenic removal. J Mater Chem A 1(3):959–965. doi:10.1039/C2TA00315E
90. Balaji T, Yokoyama T, Matsunaga H (2005) Adsorption and removal of As (V) and As (III) using Zr-loaded lysine diacetic acid chelating resin. Chemosphere 59(8):1169–1174. doi:10.1016/j.chemosphere.2004.12.007
91. Chiban M, Carja G, Lehutu G, Sinan F (2011) Equilibrium and thermodynamic studies for the removal of As (V) ions from aqueous solution using dried plants as adsorbents. Arab J Chem. doi:10.1016/j.arabjc.2011.10.002
92. Sarkar S, Blaney LM, Gupta A, Ghosh D, SenGupta AK (2008) Arsenic removal from groundwater and its safe containment in a rural environment: validation of a sustainable approach. Environ Sci Technol 42(12):4268–4273. doi:10.1021/es702556t
93. Veglio F, Beolchini F (1997) Removal of metals by biosorption: a review. Hydrometallurgy 44(3):301–316. doi:10.1016/S0304-386X(96)00059-X
94. Andrews GF, Tien C (1981) Bacterial film growth in adsorbent surfaces. AICHE J 27(3):396–403. doi:10.1002/aic.690270309, 27 396–403
95. Ozsoy HD, Kumbur H (2006) Adsorption of Cu (II) ions on cotton boll. J Hazard Mater 136(3):911–916. doi:10.1016/j.jhazmat.2006.01.035
96. Sarı A, Tuzen M (2009) Biosorption of As (III) and As (V) from aqueous solution by macrofungus (*Inonotus hispidus*) biomass: equilibrium and kinetic studies. J Hazard Mater 164(2):1372–1378. doi:10.1016/j.jhazmat.2008.09.047
97. Biswas BK, Inoue JI, Inoue K, Ghimire KN, Harada H, Ohto K, Kawakita H (2008) Adsorptive removal of As (V) and As (III) from water by a Zr (IV)-loaded orange waste gel. J Hazard Mater 154(1):1066–1074. doi:10.1016/j.jhazmat.2007.11.030
98. Hansen HK, Ribeiro A, Mateus E (2006) Biosorption of arsenic (V) with *Lessonia nigrescens*. Miner Eng 19(5):486–490. doi:10.1016/j.mineng.2005.08.018
99. Seko N, Basuki F, Tamada M, Yoshii F (2004) Rapid removal of arsenic (V) by zirconium (IV) loaded phosphoric chelate adsorbent synthesized by radiation induced graft polymerization. React Funct Polym 59(3):235–241. doi:10.1016/j.reactfunctpolym.2004.02.003
100. Muñoz JA, Gonzalo A, Valiente M (2002) Arsenic adsorption by Fe (III)-loaded open-celled cellulose sponge. Thermodynamic and selectivity aspects. Environ Sci Technol 36(15):3405–3011. doi:10.1021/es020017c
101. Mcafee BJ, Gould WD, Nadeau JC, da Costa AC (2001) Biosorption of metal ions using chitosan, chitin, and biomass of *Rhizopus oryzae*. Sep Sci Technol 36(14):3207–3022. doi:10.1081/SS-100107768
102. Matsunaga H, Yokoyama T, Eldridge RJ, Bolto BA (1996) Adsorption characteristics of arsenic (III) and arsenic (V) on iron (III)-loaded chelating resin having lysine-N α, N α-diacetic acid moiety. React Funct Polym 29(3):167–174. doi:10.1016/1381-5148(96)00041-7